Monthly Notices of the ROYAL ASTRONOMICAL SOCIETY

MNRAS **523,** 385–403 (2023)
Advance Access publication 2023 May 12

https://doi.org/10.1093/mnras/stad1392

Extreme evaporation of planets in hot thermally unstable protoplanetary discs: the case of FU Ori

Sergei Nayakshin [1]★ James E. Owen [2] and Vardan Elbakyan[1]

[1] *School of Physics and Astronomy, University of Leicester, Leicester LE1 7RH, UK*
[2] *Astrophysics Group, Department of Physics, Imperial College London, Prince Consort Rd, London SW7 2AZ, UK*

Accepted 2023 May 3. Received 2023 May 3; in original form 2023 January 27

ABSTRACT

Disc accretion rate onto low mass protostar FU Ori suddenly increased hundreds of times 85 yr ago and remains elevated to this day. We show that the sum of historic and recent observations challenges existing FU Ori models. We build a theory of a new process, Extreme Evaporation (EE) of young gas giant planets in discs with midplane temperatures of $\gtrsim 30\,000$ K. Such temperatures are reached in the inner 0.1 AU during thermal instability bursts. In our 1D time-dependent code the disc and an embedded planet interact through gravity, heat, and mass exchange. We use disc viscosity constrained by simulations and observations of dwarf novae instabilities, and we constrain planet properties with a stellar evolution code. We show that dusty gas giants born in the outer self-gravitating disc reach the innermost disc in a $\sim O(10^4)$ yr with radius of $\sim 10 R_{\rm J}$. We show that their EE rates are $\gtrsim 10^{-5} {\rm M}_\odot\,{\rm yr}^{-1}$; if this exceeds the background disc accretion activity then the system enters a planet-sourced mode. Like a stellar secondary in mass-transferring binaries, the planet becomes the dominant source of matter for the star, albeit for $\sim O(100)$ yr. We find that a $\sim$6 Jupiter mass planet evaporating in a disc fed at a time-averaged rate of $\sim 10^{-6} {\rm M}_\odot\,{\rm yr}^{-1}$ appears to explain all that we currently know about FU Ori accretion outburst. More massive planets and/or planets in older less massive discs do not experience EE process. Future FUOR modelling may constrain planet internal structure and evolution of the earliest discs.

Key words: planets and satellites: formation – planet-disc interactions – protoplanetary discs.

1 INTRODUCTION

The prototypical star FU Orionis is a member of the FUOR class (Herbig 1989), young accreting stars that undergo extreme, short increases in brightness by as much as 4–6 mag followed by slow decay on time-scales of tens to hundreds of years (for reviews see Audard et al. 2014; Fischer et al. 2022). Hartmann & Kenyon (1996) argued that most low mass stars go through the FUOR stage, experiencing bursts of accretion rate $\dot{M}_*$ as high as $10^{-4} {\rm M}_\odot\,{\rm yr}^{-1}$. While spectral characteristics of FUORs clearly implicate disc accretion as outbursts origin (e.g. see Zhu et al. 2009a), the exact physics of the disc that leads to episodic accretion remains a puzzle.

A number of authors (e.g. Hartmann & Kenyon 1985; Clarke, Lin & Pringle 1990) proposed a thermal instability (TI) scenario for FUORs [by analogy with dwarf novae outbursts (Meyer & Meyer-Hofmeister 1984; Smak 1984)]. Bell & Lin (1994) built detailed TI models for FUORs, showing that for a range of $\dot{M}_{\rm feed}$, the mass accretion rates at which the inner disc is fed from outside, the inner disc must show a cyclic behaviour, switching between a stable 'cold' branch and a stable 'hot' one. The former is characterized by disc temperatures $T \lesssim (2\text{–}3) \times 10^3$ K, when Hydrogen in the disc is neutral. The hot branch has T closer to 10^4 K, with Hydrogen in the disc fully ionized. On the cold branch, the inner disc viscosity is low, and accretion rate, $\dot{M} = \dot{M}_{\rm c}$, is lower than $\dot{M}_{\rm feed}$. This forces the gas to pile up in the disc at a distance of $R \lesssim 0.1 AU$ from the star. When enough matter accumulates, the disc heats up for Hydrogen to become ionized. On the hot branch, the viscosity is high, and the accretion rate $\dot{M}_{\rm h}$ greatly exceeds $\dot{M}_{\rm feed}$. The inner disc is thus drained onto the star in an outburst, the disc returns onto the cold branch, and the cycle repeats.

Further work (e.g. Lodato & Clarke 2004) unfortunately uncovered significant challenges for the classic TI scenario (for a review see Armitage 2015, his sections 6 and 6.1.2). To match the observed long outburst durations ($\gtrsim 100$ yr), very low values of the viscosity parameter α are required, from $\sim 10^{-4}$ to 10^{-3}. MRI simulations of the inner completely ionized disc (Davis, Stone & Pessah 2010; Simon, Beckwith & Armitage 2012; Hirose 2015; Coleman et al. 2016) and observational evidence (King, Pringle & Livio 2007; Hameury 2020) suggest much higher values, $\alpha \sim 10^{-2}$–10^{-1}. The extent of the active disc region in these models, $R_{\rm ac} \lesssim 0.1$ AU, appeared too small compared with FU Ori SED modelling and interferometric observations (which found $R_{\rm ac}$ between 0.5 and 1 AU; see Zhu et al. 2007, 2008, 2009b; Eisner & Hillenbrand 2011; Labdon et al. 2021).

Clarke & Syer (1996) and Lodato & Clarke (2004) showed that a massive gas giant planet migrating inward through the disc affects it strongly, potentially triggering TI further out in the disc than in the classic Bell & Lin (1994) models. However, the main challenge of this planet-TI model is that massive ($\sim 10\,{\rm M_J}$) gas giants are observed to be excessively rare. Using the observed mass function

★ E-mail: sn85@le.ac.uk

© 2023 The Author(s)
Published by Oxford University Press on behalf of Royal Astronomical Society. This is an Open Access article distributed under the terms of the Creative Commons Attribution License (https://creativecommons.org/licenses/by/4.0/), which permits unrestricted reuse, distribution, and reproduction in any medium, provided the original work is properly cited.

Downloaded from https://academic.oup.com/mnras/article/523/1/385/7161140 by Imperial College London Library user on 17 October 2023

of gas giants (Cumming et al. 2008), one may estimate the rate of such planets to be of order ∼0.1 per cent for FGK stars given the ∼1 per cent frequency of all hot jupiters (Santerne et al. 2016).

A clump migration scenario for FUORs was pioneered by Vorobyov & Basu (2005, 2006, 2010) who showed that massive circumstellar discs fragment due to gravitational instability (GI), producing numerous self-gravitating gas clumps. If these clumps migrate all the way to the star then intense FUOR-like accretion bursts occur. These ideas were re-invented in the field of planet formation when several authors showed that clump tidal disruptions (TD) might yield not only FUOR-like episodes of high mass accretion rate onto the stars but also leave behind sub-Jovian mass planets or solid cores (e.g. Boley et al. 2010; Nayakshin 2010; Cha & Nayakshin 2011). In relation to FUORs specifically, planet disruptions must occur in the very inner disc $R \sim (0.1–0.5)$ AU or else the outburst durations and rise times are too long compared to observations. Nayakshin & Lodato (2012) found that planets need to be radially extended (several tens of Jupiter radii, R_J) to provide better agreement with observations. However, classical FUOR outbursts are human lifetime long, and generally surprisingly steady (e.g. fig. 4 in Fischer et al. 2022). TD of planets produces short (∼ years long) spiky outbursts unless the planet is able to carve a deep gap in the disc *during* the outburst. This would only be possible is $\alpha \sim 10^{-3}$ in the inner hot disc.

An MRI activation scenario is another model for FUORs (Armitage, Livio & Pringle 2001; Zhu, Hartmann & Gammie 2009a; Bae et al. 2013, 2014). Gammie (1996) showed that for sufficiently small disc accretion rates, regions between a fraction of an AU to a few AU may be too cold (central disc temperature $T_c \lesssim 10^3$ K) to sustain a sufficient degree of ionization to support the MRI turbulence (Balbus & Hawley 1991). Only the upper layers of such discs are ionized and transport the matter towards the star at rates $\dot{M}_q \sim 10^{-8} M_\odot$ yr^{-1}. If $\dot{M}_{feed} \gg \dot{M}_q$, the matter piles up in the disc at a few AU distance from the star. Eventually, a mass reservoir with mass $\sim 0.1 M_\odot$ accumulates at these distances. Residual hydrodynamic turbulence and/or the disc's self-gravity then heats the disc enough to force alkaline metal ionization. As the dead zone viscosity increases strongly, the disc inward of ∼3 AU becomes active. A fraction of the dead zone mass is dumped onto the star; an accretion outburst results.

Recently Lykou et al. (2022) observed FU Ori via MATISSE/VLT interferometry in *L, M, N* bands and also obtained contemporaneous photometry in the number of optical and near-infra-red bands. Their results indicate that the actively accreting disc is $R_{ac} = 0.3$ AU, significantly smaller than previous estimates (see Section 3 for more discussion of this result). We show in Section 3.1 that this is an order of magnitude too small for the classical MRI-activation scenario, requiring that $\alpha \lesssim 10^{-4}$ in the hot ionized region of the disc.

Further, photometric variability of FU Ori on time-scales of days to ∼14 d led to suggestions of a massive planet orbiting the star (e.g. Powell et al. 2012). Siwak et al. (2018) used the MOST satellite data, avoiding the problems of unevenly sampled weather-depending ground-based data, firming up the ∼(10–12) d quasi-periodic variability of FU Ori with amplitude of up to 0.07 mag. For the stellar mass of $M_* = 0.6 M_\odot$ (Pérez et al. 2020), this period corresponds to a circular orbit at $R \approx 0.08$ AU.

In this paper take a closer look at the planet-TI scenario. Here we consider not only gravitational (Lodato & Clarke 2004) and mass-deposition (Nayakshin & Lodato 2012) coupling between the disc and the planet but also thermal effects of the disc onto the planet. Vazan & Helled (2012) demonstrated that very young pre-collapse gas giant planets (for terminology see Section 7.1) could be unbound by overheating in the thermal bath of the disc at distances ∼ 5–10 AU from the star. Post-collapse planets are orders of magnitude denser and hotter (Bodenheimer 1974; Graboske Jr et al. 1975), yet we show that they too are vulnerable to the thermal bath effects in the inner disc during TI bursts when they are exposed to temperatures $T \gtrsim 3 \times 10^4$ K.

In Sections 3 and 4 we argue that recent FU Ori observations challenge the MRI activation or any other scenario in which matter feeding FU Ori comes from regions larger than a fraction of an AU; a steady-state source placed inside the observed active disc region is required. In Section 5 we provide a physical model describing such a mass source. In Section 6 we present numerical experiments of increasing complexity to show how the planet and the disc interact. We then build in Section 7 a detailed model for the FU Ori outburst, constraining the disc and the planet properties tightly. A brief discussion of the model in the context of observations is given in Section 8.

2 NUMERICAL METHOD

We build on a time-dependent 1D viscously evolving disc model with an optionally embedded planet in it (Nayakshin & Lodato 2012; Nayakshin, Elbakyan & Rosotti 2022),

$$\frac{\partial \Sigma}{\partial t} = \frac{3}{R}\frac{\partial}{\partial R}\left[R^{1/2}\frac{\partial}{\partial R}\left(R^{1/2}\nu\Sigma\right)\right] - \frac{1}{R}\frac{\partial}{\partial R}\left(2\Omega^{-1}\lambda\Sigma\right) + \frac{\dot{M}_p}{2\pi R}D(R-a)\,, \quad (1)$$

where Σ is the disc surface density, Ω is the angular velocity, $\nu = \alpha c_s H$ is the Shakura & Sunyaev (1973) kinematic viscosity, c_s is the midplane sound speed, and H is the disc vertical scale height. The last two terms in equation (1) describe the angular momentum exchange between the disc and the planet via tidal torques, and the planet mass loss (that is deposited into the surrounding disc), respectively. The function $D(R-a)$ is a narrow Gaussian; when integrated over the disc area, the last term yields the planetary mass loss rate, $\dot{M}_p$, discussed in Section 5. The expressions for the planet-disc tidal torques are given in Nayakshin et al. (2022). These act on the planet (forcing it to migrate) and on the disc (modifying the disc surface density at high planet masses). A smooth transition between the type I and type II migration regimes is applied.

For quantitatively accurate results, energy equilibrium in TI-unstable inner discs needs to be solved through the vertical energy heating-cooling balance equation (e.g. Bell & Lin 1994; Hameury et al. 1998; Lasota, Dubus & Kruk 2008). These detailed models depend on the treatment of convection and assumptions about how the heating is distributed vertically. Hirose et al. (2014), Hirose (2015), and Coleman et al. (2016) perform 3D radiation-magneto-hydrodynamic simulations of discs in shearing boxes. They find that convection contributes significantly to the MRI turbulence on the hot branch and explain from first principles why discs in dwarf novae require $\alpha_{cold} \sim 0.01$ on the cold branch but $\alpha_{hot} \sim 0.1$ on the hot one (e.g. Lasota 2001; Hameury 2020). In this paper, we use the one-zone approximation to the vertical heating-cooling balance of thin discs (e.g. Lodato & Clarke 2004; Zhu, Hartmann & Gammie 2010; Bae et al. 2013; Vorobyov & Basu 2015; Kadam et al. 2020). The disc midplane temperature is solved for via

$$\frac{dT_d}{dt} = -\frac{T_d - T_{eq}}{t_{therm}} - \frac{1}{R}\frac{\partial}{\partial R}\left[T_d R v_R\right]\,, \quad (2)$$

where $t_{therm} = (\alpha\Omega)^{-1}$ is the local disc thermal time-scale, and T_{eq} is the equilibrium disc temperature found by balancing the radiative cooling rate with the local viscous heating rate. The last term in

Downloaded from https://academic.oup.com/mnras/article/523/1/385/7161140 by Imperial College London Library user on 17 October 2023

equation (2) describes radial advection of heat in the disc, with v_R the radial gas velocity in the disc.

3 WHY IS THE ACTIVE DISC SO SMALL?

Lykou et al. (2022) presented MATISSE/VLT interferometry in *L, M, N* bands and contemporaneous photometry of FU Ori in the number of optical and near-infra-red bands. Their superior spatial resolution and detailed radiative transfer modelling show an unexpectedly small radius for the hot actively accreting disc, $R_{\rm ac} \sim 0.3$ AU. The source is only marginally resolved at the longest baselines at 3.5 μm (*L* band), yielding the emitting region at 3.5 μm of $\lesssim 0.25$ AU. According to Wien's displacement law, the *L* band emission peaks at temperature ∼800 K. A steady-state self-luminous accretion disc would have this temperature at $R \approx 0.6$ AU at accretion rate $\dot{M} = 3.8 \times 10^{-5} {\rm M}_\odot\,{\rm yr}^{-1}$ (Pérez et al. 2020; in Section 3.3 the outer edge of the disc in L band in this scenario is quantified to even larger value, $R_{\rm ac} \sim 0.9$ AU). Secondly, Lykou et al. (2022) built a Monte Carlo radiative transfer model, breaking the disc into an actively accreting inner disc and a passive outer disc, and finding $R_{\rm ac} \approx 0.3$ AU.

3.1 MRI activation scenario

In quiescence, a mass reservoir exists in the disc in the 'dead zone', where the viscosity is negligible (Armitage et al. 2001). At the beginning of the outburst, the gas temperature exceeds a critical temperature, and the dead zone is ionized. One testable prediction of the model is $R_{\rm ac}$, the size of the region that participates in the outburst. The the 1D (e.g. Armitage et al. 2001; Zhu et al. 2010; Bae et al. 2013), 2D (Bae et al. 2014; Kadam et al. 2020), and 3D (Zhu, Jiang & Stone 2020) simulations of the MRI activation scenario all show that $R_{\rm ac}$ is a few AU. Here we make a simple yet robust argument that $R_{\rm ac}$ has to be that large in this scenario. Consider the hot active disc as a steady-state disc extending from the star to radius $R_{\rm ac}$. Since the luminosity of FU Ori varied little over ∼85 yr, the mass of gas in the active zone is $M_{\rm ac} \gtrsim \dot{M}_* \times 85\,{\rm yr} \geq 2 \times 10^{-3} {\rm M}_\odot$. The disc surface density at $R_{\rm ac}$ is

$$\Sigma \gtrsim \frac{M_{\rm ac}}{\pi R_{\rm ac}^2} = 5.66 \times 10^3 R_1^{-2}\ {\rm g\ cm^{-2}}\ , \tag{3}$$

where $R_1 = R_{\rm ac}/(1\ {\rm AU})$. The disc optical depth is $\tau = \kappa_{\rm R}\Sigma/2 \gg 1$, where $\kappa_{\rm R}$ is Rosseland opacity coefficient. The balance of viscous heating and radiative cooling gives

$$\frac{3GM_*\dot{M}_*}{8\pi R_{\rm ac}^3} = \frac{\sigma_{\rm B} T_{\rm d}^4}{\tau} = \sigma_{\rm B} T_{\rm d}^4 \frac{2\pi R_{\rm ac}^2}{\kappa_{\rm R} M_{\rm ac}}\ , \tag{4}$$

where $\sigma_{\rm B}$ is the Stefan–Boltzmann constant, and $T_{\rm d}$ is the disc midplane temperature. Assuming that the MRI turbulence is revived at critical temperature $T_{\rm ac} \sim 10^3$ K, we solve for the radius where $T_{\rm d}$ first falls below $T_{\rm ac}$,

$$R_{\rm ac} = \left(\frac{3GM_*\dot{M}_*}{16\pi^2\sigma_{\rm B}T_{\rm ac}^4}\kappa_{\rm R} M_{\rm ac}\right)^{1/5} = 2.8\ {\rm AU}\ \kappa_{\rm R}^{1/5} T_3^{-4/5}\ , \tag{5}$$

where $T_3 = T_{\rm ac}/(10^3\ {\rm K})$. The result does not depend on α.

Non-ideal magnetohydrodynamics simulations of protoplanetary discs (e.g. Bai & Stone 2013; Lesur 2021) indicate that the disc angular momentum transfer can be dominated by MHD winds (Blandford & Payne 1982). In this case, energy generation may occur high up in the disc atmosphere, not in the midplane. Due to this, and also due to energy losses for launching winds, such discs may be much cooler (e.g. Suzuki et al. 2016; Mori, Bai & Okuzumi 2019) than the standard turbulent viscosity ones. Could these effects be sufficiently strong to let the disc in FU Ori have midplane temperature $T_{\rm d} = T_{\rm ac} \sim 10^3$ K at the observed active disc edge, $R_{\rm ac} \approx 0.3$ AU, rather than ∼3 AU? To evaluate this idea, let $f_{\rm visc}$ be the fraction of the local accretion flow energy liberation rate dissipated due to MRI turbulence in the disc midplane. The lower $f_{\rm visc}$, the cooler the disc in the midplane, and so we can constrain the maximum $f_{\rm visc}$ that would satisfy $T_{\rm d} \lesssim T_{\rm ac}$ at 0.3 AU. In this scenario equation (4) can be re-written as

$$f_{\rm visc}\frac{3GM_*\dot{M}_*}{8\pi R_{\rm ac}^3} = \sigma_{\rm B} T_{\rm d}^4 \frac{2\pi R_{\rm ac}^2}{\kappa_{\rm R} M_{\rm ac}}\ . \tag{6}$$

With $T_{\rm d} = T_{\rm ac}$, we find

$$f_{\rm visc} \lesssim 4 \times 10^{-5} \left(\frac{R_{\rm ac}}{0.3{\rm AU}}\right)^5 T_3^4 \kappa_{\rm R}^{-1}\ . \tag{7}$$

This is vanishingly small and unlikely for an MRI-active hot inner disc. Indeed, in this case, $1 - f_{\rm visc} \sim 1$, so ≈100 per cent of the accretion flow would be due to a magnetized disc wind. If we parameterize the efficiency of angular momentum extraction via an $\alpha_{\rm dw}$ prescription (Tabone et al. 2021), then equation (7) implies that the turbulent viscosity $\alpha \sim f_{\rm visc}\alpha_{\rm dw}$ is exceedingly small. For example, at $\alpha_{\rm dw} = 0.1$ we have $\alpha \lesssim 4 \times 10^{-6}$, whereas simulations of ionized MRI-active discs show $\alpha \sim 0.1$ (e.g. Hirose et al. 2014; Hirose 2015; Zhu et al. 2020).

3.2 A mass reservoir close to the star

Let the burst be powered by a reservoir of mass located at $R_{\rm res} \ll R_{\rm ac}$, and that prior to the burst, the disc mass in the inner regions was very low compared to the reservoir mass. The outer edge of the *active* disc, in this case, is where the disc manages to spread viscously *in the outward direction* by a time t (here $t = 0$ is defined as the beginning of FU Ori outburst). By order of magnitude, this is where the viscous time $t_{\rm visc} = 1/(\alpha h^2\Omega) \approx t$, with $h = H/R$. Numerically,

$$R_{\rm ac} \approx \left[t \times \alpha h^2 (GM_*)^{1/2}\right]^{2/3} = 0.25{\rm AU} \left(\frac{\alpha}{0.03}\frac{t}{85\ {\rm yr}} h_{-1}^2\right)^{2/3} \tag{8}$$

where $h_{-1} = h/0.1$. This estimate is reasonably close to the observed value $R_{\rm ac} \approx 0.3$ AU for a realistic value of α.

3.2.1 An instantaneous mass release in the inner disc

A sudden TD of a gas giant planet may result in a sudden injection of matter into the disc. Here we add 3 $M_{\rm J}$ of gas instantaneously into the disc in a narrow ring centred on radius $R = 0.08$ AU to comply with the QPO variability seen by Siwak et al. (2018). Fig. 1 shows several snapshots of the radial profiles for the disc surface density Σ, disc midplane temperature, and the aspect ratio H/R. This model is computed for Shakura & Sunyaev (1973) viscosity parameter $\alpha = 0.01$. We also show the profile of the relative radiative cooling flux of the disc, defined as the ratio $\mathcal{F} = F/F_{\rm ss}$, where the steady-state flux $F_{\rm ss}$ is

$$F_{\rm ss} = \frac{3GM_*\dot{M}_*}{8\pi R^3} j(R)\ , \tag{9}$$

with $j(R) = 1 - (R_*/R)^{1/2}$ and stellar accretion rate $\dot{M}_* = 2 \times 10^{-5} {\rm M}_\odot\,{\rm yr}^{-1}$. $\mathcal{F}$ provides an important insight: if the model disc were in a steady state, and the mass accretion rate as inferred by Lykou et al. (2022), then $\mathcal{F} = 1$ up to the outer edge of the active disc where the flux rolls over to pre-outburst values. The black dotted

Downloaded from https://academic.oup.com/mnras/article/523/1/385/7161140 by Imperial College London Library user on 17 October 2023

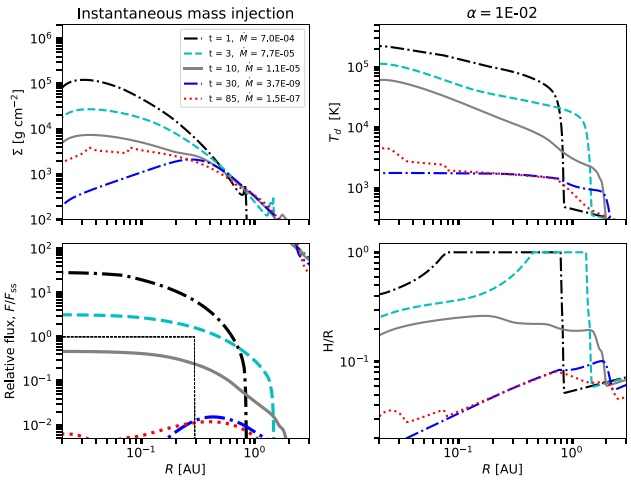


Figure 1. An instantaneous injection of $M_p = 3\,M_J$ into the inner disc (see Section 3.2.1). Shown are disc surface density Σ, midplane temperature, radiation flux normalized to the steady-state flux, and the disc aspect ratio, H/R.

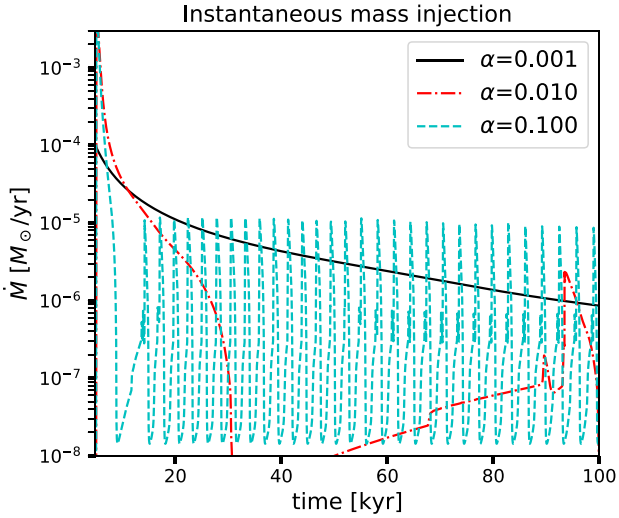


Figure 2. Stellar accretion rate for three instantaneous mass injection experiments described in Section 3.2.1.

box in the bottom left-hand panel of Fig. 1 is the observationally desirable outline of $\mathcal{F}$.

Fig. 1 shows that the disc evolves extremely rapidly. While some of the matter accretes onto the star at very high rates, other material spreads viscously outward. The inner disc is as hot as $\sim 10^5$ K, bringing H/R to values formally exceeding unity (we cap H/R at unity to prevent this unphysical situation). However, the disc cools very quickly and, within tens of years, drops from the hot stable state into the cold stable one where the disc temperature is $\sim$2000 K. This rapid $\dot{M}_*$ evolution is unlike the observed very slowly declining light curve of FU Ori. Also, the disc flux profile only briefly looks somewhat close to the desired black dotted curve.

Fig. 2 shows $\dot{M}_*$ for this toy experiment and two analogous calculations but for $\alpha = 0.001$ and $\alpha = 0.1$. None of the experiments yields an $\dot{M}_*$ similar to the observed one. The best match is obtained for an realistically low $\alpha = 0.001$, for which the relative disc flux $\mathcal{F}$, not present here for brevity, is also not consistent with the observations. For $\alpha = 0.01$, the inner disc drops into quiescence already after 30 yr of the burst, although it gets revived somewhat at later times due to TI. The disc evolves even more rapidly for $\alpha = 0.1$ and becomes TI-unstable, very unlike FU Ori.

3.2.2 An ad hoc steady state mass source

Here we experiment with a planet orbiting FU Ori at $R = 0.08$ AU which is losing mass at a fixed rate $\dot{M}_p = 2 \times 10^{-5} M_\odot\,\mathrm{yr}^{-1}$. The initial mass of the planet is $M_p = 3\,M_J$. Fig. 3 shows the disc profiles for a selection of times in the same format as in Fig. 1. Encouragingly, the relative flux $\mathcal{F}$ in Fig. 3 conforms qualitatively well to the desired step-like shape in a broad time interval, from $t \approx 10$ yr to $t = 85$ yr, and in fact, until the planet runs out of mass at $t \approx 140$ yr. Further, we repeated this steady-state planet mass loss experiment with $\alpha = 0.1$ and $\alpha = 0.001$. We found that, surprisingly, the size of the active disc in this scenario depends very little on α. Zhu et al. (2008) concluded from radiative transfer SED modelling that the accretion rate in the passive disc must drop by at least a factor of 4 compared to that in the active one. If we use the same definition for the size of the active disc here, that is, $\mathcal{F} \geq 1/4$ in the active disc, then $R_{ac} = 0.2$, 0.22, 0.32 AU for $\alpha = 10^{-3}$, 10^{-2}, and 10^{-1}, respectively, at $t = 85$ yr. All of these values are comparable to the result of Lykou et al. (2022).

The insensitivity of R_{ac} to the value of α stems from the fact that h in equation (8) actually anticorrelates with α. Fig. 4 shows the relative radiative fluxes of the three α models in the top panel, and the local disc viscous time in the bottom panel at $t = 85$ yr, the current age of FU Ori outburst. For all the values of α the viscous time at $R \geq 0.3$ AU is longer than 85 yr. Therefore, the material outflowing to larger radii has not had time to reach beyond 0.3 AU.

3.3 Cumulative disc fluxes in L band

Lykou et al. (2022) marginally resolve FU Ori in the L band, concluding that the emission in FU Ori is neither a point source nor a region with R much larger than 0.3 AU. They find that about 1/4 of the flux in the L band comes from the passive disc at $R > 0.3$ AU. In this paper we do not model this reprocessing, and so we focus here just on the L band emission by the active disc. In Fig. 5, the observed radiative flux of actively accreting region in FU Ori disc at 3.5 μm (Lykou et al. 2022) is shown with the horizontal dotted line. For simplicity we assume the disc to emit as a local blackbody, then calculate the local emitted flux at L band, and compute the cumulative disc flux in this band at the observer as a function of the radius in the disc. In Fig. 5, cumulative disc fluxes are shown for the following models: instantaneous mass release (TD; red lines, Section 3.2.1), the steady state mass loss [steady state evaporation, Extreme Evaporation (EE); blue lines, see Section 3.2.2] by the planet orbiting at $R = 0.08$ AU; and a steady-state disc with mass accretion rate $\dot{M} = 2 \times 10^{-5} M_\odot\,\mathrm{yr}^{-1}$ (black line). The model fluxes are shown at different times. The vertical dotted line shows the inferred active disc size in FU Ori (Lykou et al. 2022). The cumulative flux shown in the figure must saturate at the intersection of vertical and horizontal dotted lines for the model fluxes to match the observations.

The cumulative L band flux of the steady state model is higher than observed by a factor of 2.5. The radius of flux saturation in this model is a factor of 3 larger than observed R_{ac}. The model disc is too bright and too large.[1]

[1]After this paper was accepted to publication, Bourdarot et al. (2023) presented interferrometric observations of FU Ori in H and K NIR bands that also find an active disc radius of $\sim$0.3 AU. While these results confirm

Downloaded from https://academic.oup.com/mnras/article/523/1/385/7161140 by Imperial College London Library user on 17 October 2023

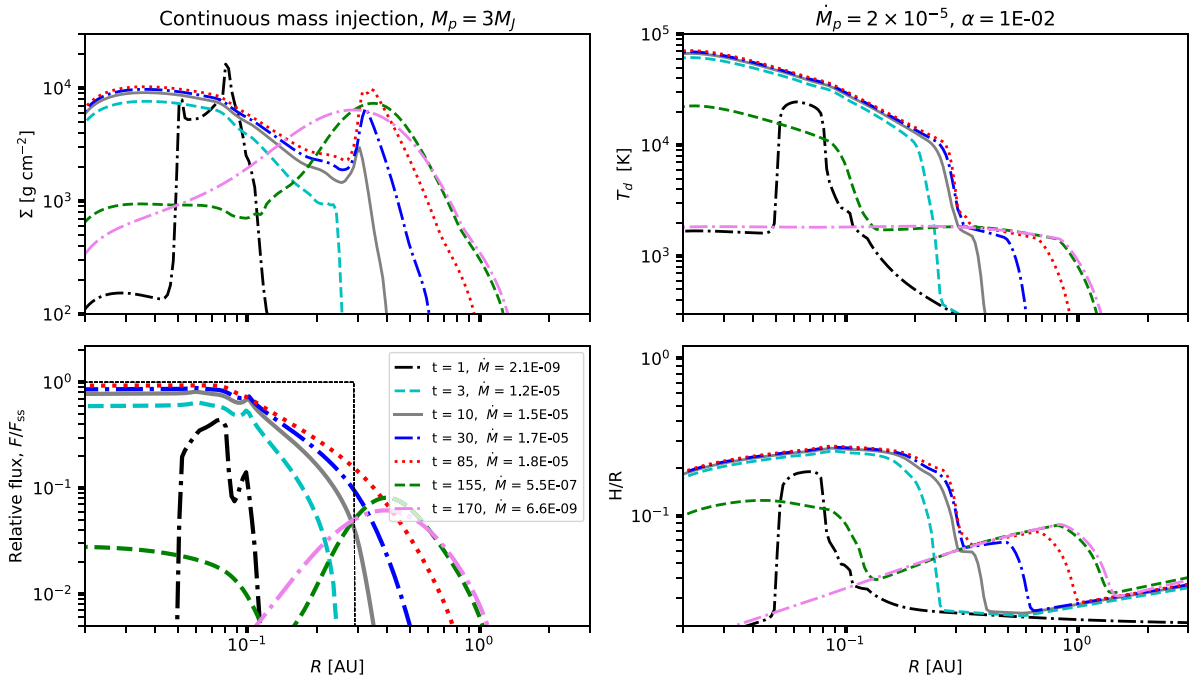


Figure 3. Same as Fig. 1 but now the planet lose mass at a constant rate of $\dot{M}_{\rm p} = 2 \times 10^{-5} {\rm M}_\odot\,{\rm yr}^{-1}$. The relative flux $\mathcal{F}$ is close to the desired shape for ∼90 per cent of the outburst duration.

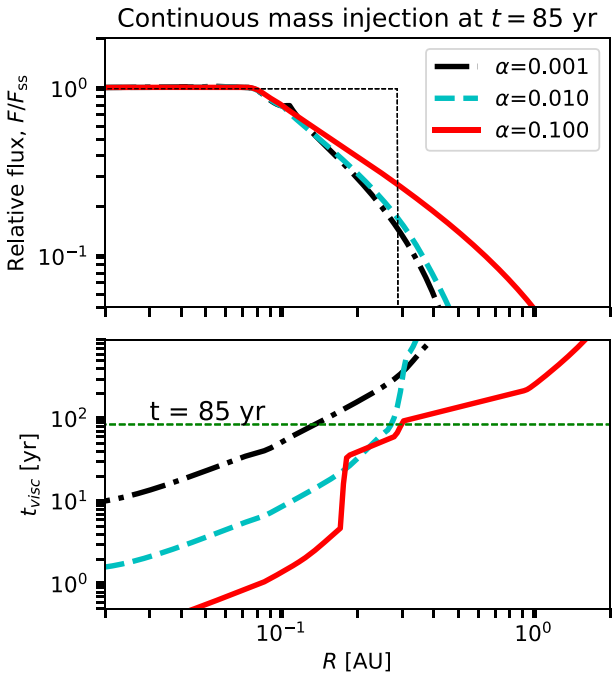


Figure 4. Comparison of relative disc fluxes (equation 9) and the viscous time vs radius for the different values of α in the steady-state mass source model (Section 3.2.2.) Note that for all α the size of the active disc is 0.2–0.3 AU, close to the observed value.

Lykou et al. (2022) findings in the L band, interestingly the authors find that an MRI activation based scenario (in the spirit of Armitage et al. 2001) fit the disc size quite well. This to some degree disagrees with our conclusions here. We intend to investigate this disagreement further in future work.

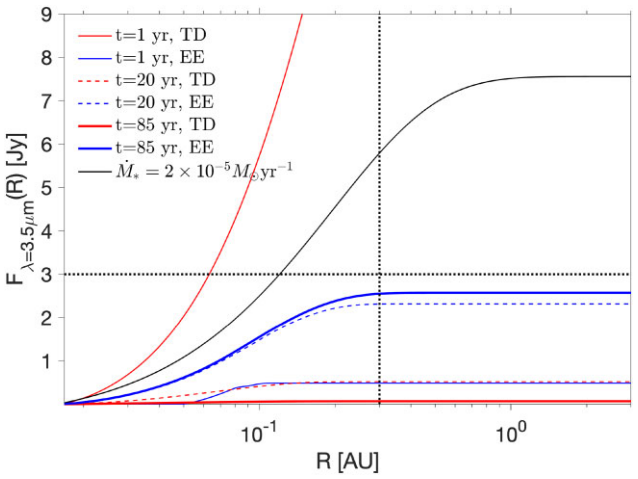


Figure 5. Radial dependence of cumulative radiative flux in the models presented in Section 3.2.1 (red lines), Section 3.2.2 (blue lines), and in a steady state disc model with a constant stellar mass accretion rate $\dot{M}_* = 2 \times 10^{-5} {\rm M}_\odot\,{\rm yr}^{-1}$ (black line). The vertical dotted line shows the active region size in FU Ori disc, $R = 0.3$ AU. The horizontal dotted line shows the observed disc radiative fluxes at 3.5 μm for FU Ori. (Lykou et al. 2022).

In the TD model, the flux spikes dramatically at early times when the cumulative flux is about an order of magnitude too high. During the next ∼30 yr, the flux decreases rapidly. The flux saturation radius in the model at $t = 30$ yr is 0.3–0.4 AU, close to the size of active disc size in FU Ori. However, the flux stays close to the observed values for only a short period of time and then continues to plummet, becoming by a factor of 50 too low (thick red line) at $t = 85$ yr. Thus, the model is able to reproduce the fluxes and active disc size for only a few years. It also contradicts the observed weak evolution of B and V band fluxes (e.g. Clarke et al. 2005).

Downloaded from https://academic.oup.com/mnras/article/523/1/385/7161140 by Imperial College London Library user on 17 October 2023

In the EE model, the radiative flux gradually increases after the planet starts losing mass. The growth slows down over time and reaches 2.6 Jy at $t = 85$ yr, being consistent with the observed value. Flux saturation is at $R \sim 0.3$ AU. Unlike the TD model, disc flux in the EE model spends many decades close to the observed fluxes of FU Ori.

4 WHY NO TI IN FU ORI?

The FU Ori lightcurve has been steadily declining over almost 100 yr. While TI cannot provide a good match to the data, should we not expect TI instability to operate and make FU Ori vary strongly and non-monotonically over this long a time-scale? The physics of TI applies to any accretion disc system exceeding the minimum accretion rate $\dot{M}_{\rm min}$ (Bell & Lin 1994; Lasota 2001) for instability. Importantly, $\dot{M}_{\rm min}$ is independent of the value of α because it is set by the ionization conditions of Hydrogen (Hameury 2020). Lasota et al. (2008) show that for a star of mass $m_* {\rm M}_\odot$ with a Solar composition disc, TI operates inside a radius in the disc $R_{-1} = R/(0.1\ {\rm AU})$ if $\dot{M}_{\rm feed}$ exceeds

$$\dot{M}_{\rm min} = 1.7 \times 10^{-5} \frac{{\rm M}_\odot}{\rm year}\ R_{-1}^{2.58} m_*^{-0.85}\ . \tag{10}$$

Currently $\dot{M}$ in FU Ori is a few$\times 10^{-5} {\rm M}_\odot\ {\rm yr}^{-1}$ (Lykou et al. 2022), and historical data indicate it may have been a factor of 2–3 higher in the past (e.g. Clarke et al. 2005). Based on equation (10), we expect the inner ∼0.2 AU of the disc in FU Ori to be unstable to TI. $\dot{M}$ through the inner disc of FU Ori *should have* varied by orders of magnitude during the past 85 yr, but it has not.

A clue is provided by the experiments in Section 3.2.2 with an *ad hoc* steady-state mass source located at 0.08 AU. We found in Section 3.2.2 that, whatever the value of α, the accretion rate onto the star is steady despite the planet injecting the mass into the disc at a rate $\sim 2 \times 10^{-5} {\rm M}_\odot\ {\rm yr}^{-1}$. This $\dot{M}_{\rm feed}$ makes a conventional outside-in fed disc unstable. Evidently, feeding the disc from inside the unstable region may render it steady.

To explore this further, we run a series of numerical experiments set up similarly to those in Section 3.2.2 but for a range of source locations. In parallel to that, we employ the following prescription for the behaviour of α with the disc temperature,

$$\ln \alpha = \ln \alpha_{\rm cold} + \frac{\ln \alpha_{\rm hot} - \ln \alpha_{\rm cold}}{1 + (T_{\rm cr}/T)^8}, \tag{11}$$

where $T_{\rm cr} = 2.5 \times 10^4$ K is a critical temperature. This anszat, with $\alpha_{\rm cold} = 0.01$ and $\alpha_{\rm hot} = 0.1$, was proposed by Hameury et al. (1998) and was found to work relatively well for both observations (e.g. Lasota 2001) and first-principle simulations of TI in discs (Hirose et al. 2014; Hirose 2015).

We begin with a disc in steady-state at all radii inside the computational domain, transporting the matter towards the star at a very low accretion rate, $\dot{M} = 10^{-9} {\rm M}_\odot\ {\rm yr}^{-1}$. A source of matter losing mass at rate $\dot{M}_{\rm p} = 2 \times 10^{-5} {\rm M}_\odot\ {\rm yr}^{-1}$ is then placed into the disc at radius $a_{\rm s}$, where $a_{\rm s}$ is a parameter that ranges from 0.06 to 1.2 AU for different runs. As we aim to reproduce a quasi-steady accretion rate observed in FU Ori, we run the simulations long enough for the matter lost by the source to reach the star plus a few thousand years. This ensures that the time average accretion rate onto the star by the end of these experiments is close to $\dot{M}_{\rm feed}$.

Fig. 6 shows stellar $\dot{M}$ versus time for such experiments, with the respective value of $a_{\rm s}$ shown in the legend. For $a_{\rm s} = 0.06$ and 0.16 AU, accretion is steady, whereas for $a_{\rm s} = 0.44$ and 1.2 AU TI is clearly present; we can rule such models out. To characterize

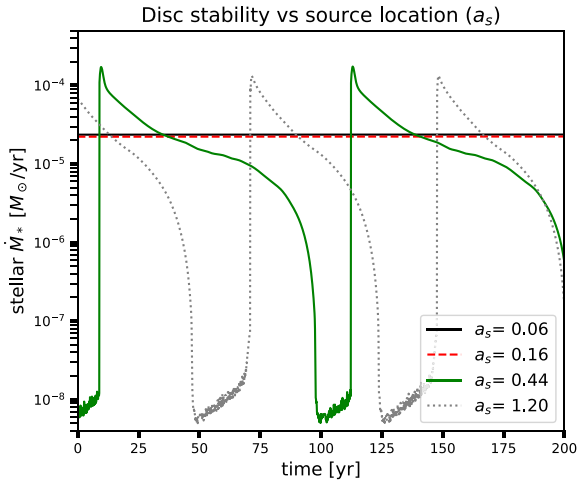


Figure 6. Stellar accretion rate $\dot{M}_*$ versus time for experiments with an *ad hoc* steady-state source placed at different radial locations $a_{\rm s}$ as shown in the legend. Note that only when the source is located sufficiently close to the star $\dot{M}_*$ is steady.

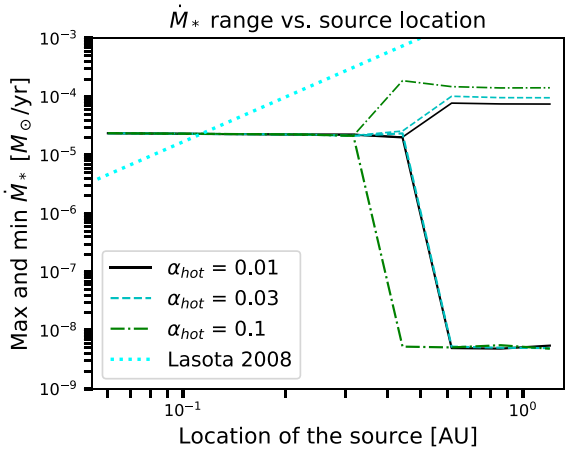


Figure 7. The maximum and minimum accretion rate onto the star (cf. Fig. 6) versus the source of matter location. To explain the long-term stability of FU Ori, the source must be located inside ∼0.3 AU. See text in Section 4 for detail.

the variability properties of such experiments versus $a_{\rm s}$, we measure the minimum and maximum accretion rates onto the star and plot these in Fig. 7. To evaluate the dependence of the results on the α prescription, we also considered two other values of $\alpha_{\rm hot} = 0.01$ (same as $\alpha_{\rm cold}$), and $\alpha_{\rm hot} = 0.03$, and plot the results in Fig. 7. The figure shows that disc accretion onto the star is in steady-state if the source of matter is located at $a_{\rm s} \lesssim 0.3$ AU, although there is a weak dependence on the α prescription. We also show in Fig. 7 the critical accretion rate $\dot{M}_{\rm min}$ given by equation (10). If our disc behaved as the local disc S-curves predict (Lasota et al. 2008) then we would expect $\dot{M}_*$ to be stable only for $a_{\rm s} \lesssim 0.12$ AU rather than $a_{\rm s} \sim 0.3$ AU. It is possible that our one vertical zone approximation is insufficiently accurate compared to the more detailed vertical balance models of Lasota et al. (2008). Alternatively, the inner disc injection of mass and the non-local terms present in our modelling may be important. In any event, these experiments show that a quasi-steady source of matter placed inside the region $R \lesssim (0.1 - 0.3)$ AU from the star results in a steady $\dot{M}_*$. On the other hand, if the matter is introduced

Downloaded from https://academic.oup.com/mnras/article/523/1/385/7161140 by Imperial College London Library user on 17 October 2023

into the disc at larger distances, then we should expect FU Ori to have shown variability in $\dot{M}_*$ by many magnitudes since the beginning of the outburst, but it has been remarkably steady over ∼85 yr (Clarke et al. 2005; Lykou et al. 2022).

The absence of TI in FU Ori challenges the MRI activation scenario directly because the 'source' of the matter input into the active disc in this model is the inner edge of the dead zone, i.e. ≈2–3 AU (Section 3.1). 2D simulations of the FU Ori hot disc by Zhu et al. (2009c) confirm this conclusion. Such simulations are very expensive numerically when they cover more than one decade in radius, and so one often sets the inner region to exclude the TI-unstable zone. However, Zhu et al. (2009c) found that when the inner ∼0.1 AU of the disc is resolved in the simulations then TI does appear and leads to a significant and rapid variability in $\dot{M}$ on the star.

5 EXTREME EVAPORATION OF PLANETS

5.1 Preliminaries: thermal boil off

Owen & Wu (2016) studied thermally driven Parker winds from ∼(1–10) Earth-mass planets exposed to irradiation from the central star. The two essential radial scales for the problem are the planet radius R_p and the Bondi radius,

$$R_\mathrm{B} = \frac{GM_\mathrm{p}}{2c_s^2} \approx 21 R_\mathrm{J}\, m_3 T_4^{-1}\ , \tag{12}$$

where $T_4 = T_\mathrm{h}/(10^4\mathrm{K})$ where T_h is the temperature of the hot thermal bath surrounding the planet, and $m_3 = M_\mathrm{p}/(3\,\mathrm{M_J})$. As we will assume that the outer layers of the planet are warmed up to T_h, R_B is where the planet's gas is no longer thermally bound to it and can escape it.

Simple estimates (fig. 1 in Nayakshin 2010), semi-analytical models (e.g.the right-hand panel in fig. 4 of Humphries et al. 2019), and 3D numerical simulations (e.g. Vorobyov & Basu 2006; Boley et al. 2010; Fletcher et al. 2019) show that gas giants born at ∼50 AU by GI may migrate into the inner AU in $\sim 10^4$ yr. The radius of such planets can be as large as $R_\mathrm{p} \sim O(10)R_\mathrm{J}$; cf. Section 7.1 for detail.

Let us consider the case when R_p is smaller than the Hill radius R_H of the planet, $R_\mathrm{H} = a\left(\frac{M_\mathrm{p}}{3M_*}\right)^{1/3} \approx 25 R_\mathrm{J}\, a_{-1} m_3^{1/3}$, where $a_{-1} = a/(0.1\,\mathrm{AU})$, and we assumed $M_* = 0.6\mathrm{M}_\odot$. Owen & Wu (2016) show that in the 'boil-off' regime $R_\mathrm{p} \ll R_\mathrm{B}$, the mass outflow rate is

$$\dot{M}_\mathrm{p} = 4\pi R_\mathrm{p}^2 \rho_\mathrm{surf} v_\mathrm{out}\ , \sim 6\times 10^{-8}\frac{\mathrm{M}_\odot}{\mathrm{yr}} m_3 T_4^{-1/2}\frac{v_\mathrm{out}}{c_\mathrm{h}}\kappa_\mathrm{R}^{-1}\ , \tag{13}$$

where ρ_surf is the photospheric density, κ_R is Rosseland opacity, and v_out is strongly subsonic with respect to the sound speed $c_\mathrm{h} = (k_b T_h/\mu)^{1/2} \approx 10\, T_4^{1/2}$ km/s. While very important for super-Earth planets, such mass loss rates are very small in terms of FU Ori phenomenon.

5.2 Optically thick energy limited outflow

In isolation, photospheric temperatures of the youngest giant planets and brown dwarfs, T_ph, is in the range $\sim(1\text{–}3)\times 10^3$ K (Bodenheimer 1974; Bodenheimer et al. 1980; Burrows et al. 1997). Consider the situation where the temperature of the external medium in which the planet is bathed suddenly increases by a large factor to $T_\mathrm{h} > 10^4$ K and the planet finds itself in the regime $R_\mathrm{B} < R_\mathrm{p} < R_\mathrm{H}$. As $T_\mathrm{h} \gg T_\mathrm{ph}$, radiation diffuses *into* the planet, heating its outer layers to $\sim T_\mathrm{h}$, making them unbound and launching an outflow.

We seek a steady-state solution in which the mechanical luminosity of the outflow is equal to the radiation energy flux entering the planet. As the flow is optically thick, radiation and gas are in thermodynamic equilibrium. In the outflow region, the gas temperature is a monotonically increasing function of radius R counted in this section from the planet centre, and the radiation flux, F_rad is directed into the planet.

Outflows from stars and planets are often supersonic at large distances. Here, however, the flow is unlikely to be supersonic. If it were supersonic at large distances, there would be a shock where the outflow ram pressure meets sufficient resistance from the surrounding disc. The shock would not be isothermal as the disc is optically thick. The gas would be heated to temperature $T \gg T_\mathrm{h}$. But then the radiation flux at that point would change sign and be positive. The outflow would be cut off from its ultimate energy source, the hot disc surrounding the planet, and would therefore shut down.

The steady-state energy equation for an evaporative flow is (cf. Cowie & McKee 1977)

$$\vec{\nabla}\cdot\rho\vec{v}\left(\frac{5}{2}c_\mathrm{s}^2 + \frac{v^2}{2}\right) + \vec{\nabla}\cdot\vec{F}_\mathrm{rad} = 0\ , \tag{14}$$

where c_s and v are the local sound and speed velocity of the gas, respectively.

In spherical symmetry,

$$F_\mathrm{rad}(R) = -\frac{16}{3}\frac{\sigma_B T^3}{\kappa_\mathrm{R}\rho}\frac{\mathrm{d}T}{\mathrm{d}R}\ , \tag{15}$$

and equation (14) can be integrated,

$$\rho v\left(\frac{5}{2}c_\mathrm{s}^2 + \frac{v^2}{2}\right) = \frac{16}{3}\frac{\sigma_B T^3}{\kappa_\mathrm{R}\rho}\frac{\mathrm{d}T}{\mathrm{d}R}\ . \tag{16}$$

Here the constant of integration was set to zero due to boundary conditions at infinity: the radiation flux entering the planet from the disc [the right hand side of equation (16)] is exactly equal to the outflow energy flux (the left-hand side). Multiplying both sides of the equation by $4\pi R^2$ and identifying $\dot{M}_\mathrm{p} = 4\pi R^2\rho v = \mathrm{const}$ as an unknown eigenvalue of the problem, we have

$$\dot{M}_\mathrm{p}\left(\frac{5}{2}c_\mathrm{s}^2 + \frac{v^2}{2}\right) = \frac{64\pi}{3}\frac{\sigma_B R^2 T^3}{\kappa_\mathrm{R}\rho}\frac{\mathrm{d}T}{\mathrm{d}R}\ . \tag{17}$$

We shall make a simplifying assumption that $v = c_\mathrm{s}$ everywhere in the flow. Since $R_\mathrm{p} > R_\mathrm{B}$ and the flow is thermally launched, it has enough thermal energy to escape everywhere, yet it is not likely to be accelerated much above c_s since it is thermally driven. The density ρ is eliminated through $\rho = \dot{M}_\mathrm{p}/(4\pi R^2 c_\mathrm{s})$, and

$$\dot{M}_\mathrm{p}^2 = \frac{256\pi^2}{9}\frac{\sigma_B R^4 T^{5/2}}{\kappa_\mathrm{R}}\left(\frac{\mu}{k_b}\right)^{1/2}\frac{\mathrm{d}T}{\mathrm{d}R}\ . \tag{18}$$

The opacity κ_R is a complicated function of density ρ and temperature, and therefore equation (18) cannot be solved analytically.

5.2.1 *Order of magnitude estimate*

Let us first estimate $\dot{M}_\mathrm{p}$. The outflow is launched in the region close to the planet's surface, so by the order of magnitude $R \sim R_\mathrm{p}$, $\mathrm{d}T/\mathrm{d}R \sim (T_\mathrm{h} - T_\mathrm{ph})/R_\mathrm{p} \sim T_\mathrm{h}/R_\mathrm{p}$, and $T \sim T_\mathrm{h}$. With this, we obtain the 'characteristic' mass loss rate

$$\dot{M}_\mathrm{char} = \frac{16\pi}{3}\left(\frac{\sigma_B}{\kappa_\mathrm{R}}\right)^{1/2}\left(\frac{\mu}{k_b}\right)^{1/4} R_\mathrm{p}^{3/2} T_\mathrm{h}^{7/4}\ . \tag{19}$$

Numerically, with $\mu = 0.6 m_p$,

$$\dot{M}_\mathrm{char} = 2.25\times 10^{-6}\frac{\mathrm{M}_\odot}{\mathrm{year}}\kappa_\mathrm{R}^{-1/2}\left(\frac{R_\mathrm{p}}{10R_J}\right)^{3/2} T_4^{7/4}\ . \tag{20}$$

Downloaded from https://academic.oup.com/mnras/article/523/1/385/7161140 by Imperial College London Library user on 17 October 2023

For $T_4 \sim$ a few, this is of the order of the accretion rate in the inner active disc of FU Ori. Note that equation (19) depends on opacity κ_R, assumed constant throughout the flow in this estimate. Even in this case, to find $\dot{M}_p$ at a given T_h, one needs to solve equation (19) for $\dot{M}_{char}$ iteratively, by adjusting the estimate of $\rho = \dot{M}_{char}/(4\pi R^2 c_s)$ and using this in opacity κ_R. We find that in general $\kappa_R \sim 10$ for the problem at hand.

5.2.2 An approximate analytical solution

In this section, we continue with our approximation that $\kappa_R = \text{const}$. This then allows us to integrate equation (18) in a closed form. The constant of integration follows from demanding $T(R_p) = T_{ph}$,

$$\frac{512\pi^2}{3}\frac{\sigma_B}{\kappa_R}\left(\frac{\mu}{k_b}\right)^{1/2}(T^{7/2} - T_{ph}^{7/2}) = \dot{M}_p^2\left(\frac{1}{R_p^3} - \frac{1}{R^3}\right). \quad (21)$$

The value of $\dot{M}_p$ is now found by demanding $T(\infty) = T_h$:

$$\dot{M}_p = 16\pi\sqrt{\frac{2}{3}}\left(\frac{\mu}{k_B}\right)^{1/4}\left(\frac{\sigma_B}{\kappa_R}\right)^{1/2} R_p^{3/2}\left(T_h^{7/4} - T_{ph}^{7/4}\right). \quad (22)$$

If we neglect $T_{ph} \ll T_h$ in this equation then it is exactly $\sqrt{6} = 2.44$ times larger than $\dot{M}_{char}$. Numerically,

$$\dot{M}_p = \dot{M}_{ee} = 5.5\times10^{-6}\frac{M_\odot}{\text{year}}\left(\frac{R_p}{10R_J}\right)^{3/2}\frac{T_4^{7/4}}{\kappa_R^{1/2}}\left(1 - \frac{T_{ph}^{7/4}}{T_h^{7/4}}\right) \quad (23)$$

5.2.3 Radiation diffusion limiter on $\dot{M}_p$

Throughout the derivation in Sections 5.2.1 and 5.2.2, we neglected the fact that radiation diffuses into the planet at a finite speed c_{diff}. We can formally define this speed through $u_{rad}c_{diff} = |F_{rad}|$, where $u_{rad} = a_{rad}T^4$ is the blackbody radiation energy density, obtaining

$$c_{diff} = c\,\frac{d\ln T^{4/3}}{d\tau} \approx \frac{c}{\tau_{out}}. \quad (24)$$

Here we used the fact that $T_h \gg T_{ph}$. We shall now recognize the fact that radiation is also advected outward with the flow at velocity v_{out}. If $v_{out} > c_{diff}$, then external radiation will not reach the interior layers of the planet and the outflow will shut down. We must therefore require that $c_{diff} \gtrsim v_{out}$, or equivalently,

$$\tau_{out} = \frac{\kappa_R\dot{M}_p}{4\pi R_p v_{out}} \le \frac{c}{v_{out}}, \quad (25)$$

which evidently results in an upper limit,

$$\dot{M}_p \le \dot{M}_{max} = \frac{4\pi c R_p}{\kappa_R} = 4.2\times10^{-4}\frac{M_\odot}{\text{year}}\kappa_R^{-1}\frac{R_p}{10R_J}. \quad (26)$$

More formally, and more accurately, a similar result is derived by including the radiation advection term into the left-hand side of equation (16), which then becomes

$$\dot{M}_p\left(\frac{5}{2}c_s^2 + \frac{v^2}{2} + \frac{E_{rad}}{\rho}\right), \quad (27)$$

where the radiation energy density $E_{rad} = a_r T^4$. When the outflow is radiation pressure dominated, the E_{rad}/ρ term in equation (27) is the dominant one. Upon neglecting the gas energy density terms one can derive the temperature structure of such a flow

$$\ln T = \ln T_{ph} + \frac{3\kappa_R}{16\pi c}\dot{M}_p\left(\frac{1}{R_p} - \frac{1}{R}\right). \quad (28)$$

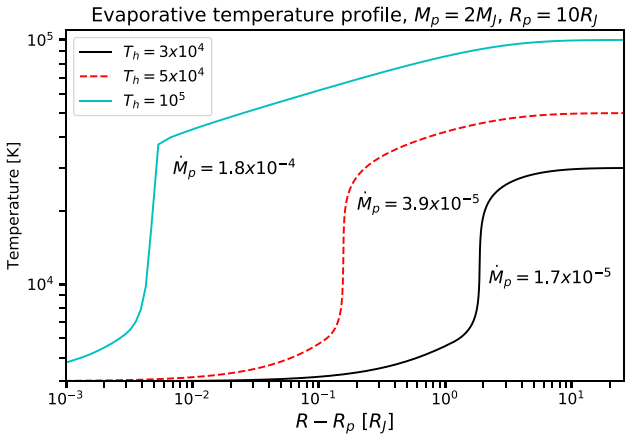


Figure 8. Radial temperature profiles for the EE of the planet computed as described in Section 5.2.4. Three values of the hot bath temperature T_h are considered.

Setting $T = T_h$ at $R = \infty$, we have

$$\dot{M}_{diff} = \frac{16\pi c R_p}{3\kappa_R}\ln\left(\frac{T_h}{T_{ph}}\right) = \frac{5.6\times10^{-4}}{\kappa_R}\frac{M_\odot}{\text{year}}\frac{R_p}{10R_J}\ln\left(\frac{T_h}{T_{ph}}\right) \quad (29)$$

As $\ln(T_h/T_{ph}) \sim 2 - 4$, this results in pre-factor in equation (29) of $\sim (1 \div 2)\times10^{-3}M_\odot\,\text{yr}^{-1}$. We see that the radiation diffusion limit to $\dot{M}_p$ is usually significantly larger than equation (23), unless both $T_4 \gg 1$ and $\kappa_R \gg 1$.

5.2.4 Numerical solution

Lastly, we perform direct numerical integration of equation (18), not assuming now that $\kappa_R = \text{const}$, for a given set of problem parameters, that is, M_p, R_p, and T_h. In doing so we first guess a value for $\dot{M}_p$. We then equation (18) outward in small increments of R to ensure small changes in T in every step, starting at $R = R_p$, and setting $T(R_p) = 4\times10^3$ K. This temperature is still much lower than T_h and is large enough so that H_2 molecules would be largely dissociated. For a more accurate solution, one needs to include H_2 dissociation and H ionization, but we expect only a minor correction since the gain in the specific internal energy of gas as it warms up to $T_h \sim$ a few $\times\,10^4$ K far outweighs these additional energy sinks. Note that radiation flux drops as $1/R^2$ at large radii from the planet since $4\pi R^2 F(R) = \text{const}$ for a steady state solution, implying that $dT/dR \to 0$, and hence $T(R)$ tends to a constant ($T(\infty)$) at $R \to \infty$. In general $T(\infty) \ne T_h$; we then iterated on the value of $\dot{M}_p$ until we matched the outer boundary condition, $T(\infty) = T_h$ at $R \gg R_H$.

Fig. 8 shows $T(R)$ profiles for $R_p = 10R_J$, $M_p = 2\,M_J$ and three different values of T_h. We can see that the larger T_h, the steeper the temperature rise from the planet's surface. The width of the radial zone where the temperature suddenly increases to above 10^4 K is always much smaller than a fraction of R_J, which is very small compared to the planet's radius. Fig. 8 also shows the planet mass loss rates derived through this numerical procedure. Encouragingly, these values are within ~20 per cent of the approximate $\dot{M}_p$ given by equation (23) (we remind the reader that one still needs to iterate on κ_R in that equation to find an accurate expression for the mass loss rate, although $\kappa_R \approx 10$ usually gives a result accurate to within a factor of 2).

Fig. 9 shows $\dot{M}_p$ obtained from equation (23) versus T_h for a selection of planet parameters. In the left-hand panel of the figure, we show planets with $R_p = 10R_J$ but with three different values of

Downloaded from https://academic.oup.com/mnras/article/523/1/385/7161140 by Imperial College London Library user on 17 October 2023

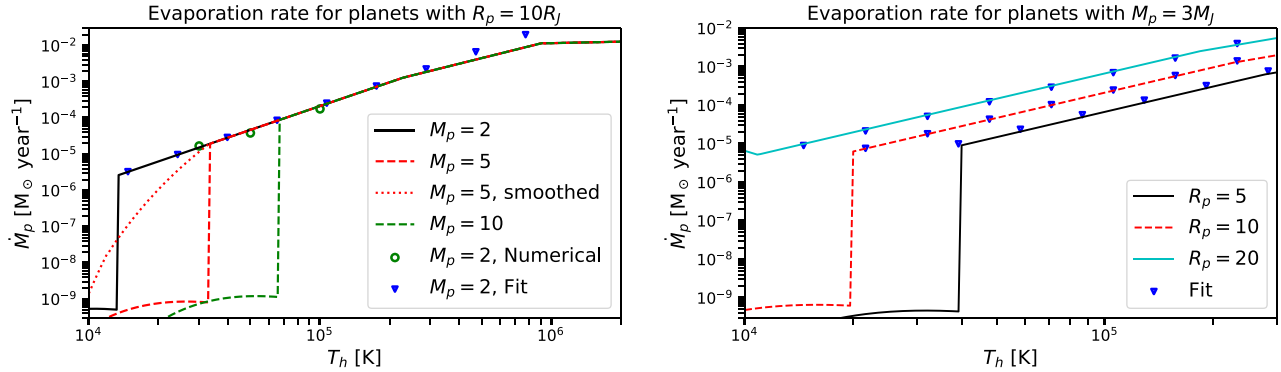


Figure 9. Dependence of planet EE rates computed via equations (13) and (23) on the surrounding gas temperature for a selection of planet parameters. Left: Fixed planet radius, $R_\mathrm{p} = 10R_J$, and varying M_p. The smoothed evaporation model is discussed in Section 6.2. The green circles and blue triangles show the numerical solution (Section 5.2.4) and the approximation via equation (30), respectively. Right: Same but for a fixed M_p and varying R_p.

M_p. Note that since we neglected planet gravity (recall that $R > R_\mathrm{p} > R_\mathrm{B}$ so the gas is not bound to the planet), there is no dependence of $\dot{M}_\mathrm{p}$ on M_p, except at relatively low T_h. In particular, if T_h is low, $R_\mathrm{B} > R_\mathrm{p}$, and so extreme evaporation does not take place. In that case, we use the Parker wind solution which yields much lower values of $\dot{M}_\mathrm{p} \sim 10^{-9}\mathrm{M}_\odot\,\mathrm{yr}^{-1}$. The three green circles in the left-hand panel of Fig. 9 correspond to the numerical solutions obtained for $M_\mathrm{p} = 2\,\mathrm{M_J}$ and plotted in Fig. 8. Therefore, in the rest of the paper, we shall use equation (23) for a numerically quick evaluation of $\dot{M}_\mathrm{p}$. For analytical purposes we also note the following numerical fit that works quite well:

$$\dot{M}_\mathrm{p} = 1.4 \times 10^{-6} \frac{\mathrm{M}_\odot}{\mathrm{year}} \left(\frac{T_\mathrm{h}}{10^4\mathrm{K}}\right)^{\xi_p} \left(\frac{R_\mathrm{p}}{10R_\mathrm{J}}\right)^{3/2}, \qquad (30)$$

(blue triangles in Fig. 9) where $\xi_p = 2.2$, until the radiation diffusion limit (equation 26) is reached.

6 IDEALISED DISC-PLANET CO-EVOLUTION

In this section we start with idealized experiments that inject the planet into the inner disc and neglects its radial migration. In this section the planet 'feels' the surrounding disc's heat but not its tidal torque; the disc also feels no torques from the planet but receives the mass lost by the planet [in terms of equation (1), the second term on the right is set to zero but the last term is on]. Unrealistically we also keep $M_\mathrm{p} = \mathrm{const}$ in this section; this is relaxed in Section 7.

6.1 FUOR ignition, and two system modes

When do planet-disc systems produce FUOR-like behaviour? To investigate this we start with a fixed $\alpha = 5 \times 10^{-3}$ planet-free disc fed at $\dot{M}_\mathrm{feed} = 10^{-7}\mathrm{M}_\odot\,\mathrm{yr}^{-1}$ at infinity. At this $\dot{M}_\mathrm{feed}$ the disc switches between quiescent periods with $\dot{M}_\mathrm{q} \sim 10^{-8}\mathrm{M}_\odot\,\mathrm{yr}^{-1}$ lasting ∼70 yr, and outbursts with $\dot{M} = \dot{M}_\mathrm{b} \sim 10^{-6}\mathrm{M}_\odot\,\mathrm{yr}^{-1}$ lasting ∼10 yr. We then inject a planet with mass $M_\mathrm{p} = 3\,\mathrm{M_J}$ into the disc at $R = 0.08$ after 300 yr of its planet-free evolution.

In quiescence, $T \lesssim 2 \times 10^3$ K, and planet evaporation is negligible. However, at the peak of TI outbursts the EE rate may be comparable to or even exceed $\dot{M}_\mathrm{b}$. We shall now see that if $\dot{M}_\mathrm{p} < \dot{M}_\mathrm{b}$ then the planet is in the 'disc-controlled' mode, in which the planet simply follows the local disc conditions as it goes through the TI cycle. In the opposite case, if during a TI outburst $\dot{M}_\mathrm{p} > \dot{M}_\mathrm{b}$, then the planet-disc system becomes highly non-linear. The planet becomes the main source of matter in the inner disc, exceeding the mass supply from the outside planetary orbit. We call this system mode 'planet-sourced'. As mass is released by the planet, the disc heats up, so $\dot{M}_\mathrm{p}$ increases further; an FUOR-like outburst with accretion rate $\approx \dot{M}_\mathrm{p} \gg \dot{M}_\mathrm{b}$ is ignited.

To delineate the two modes of the system we perform experiments for a range of R_p, finding that there exists a critical value, R_cr. For the parameters chosen, $R_\mathrm{cr} \approx 10.57R_J$. Fig. 10 shows the accretion rate onto the star (solid curves) and the planet mass loss rates, $\dot{M}_\mathrm{p}$ (circles) in the top panels, and the disc temperature (called planet irradiation temperature in the panels) at the location of the planet in the bottom panels. The left- and right-hand panels show the same curves, but the right-hand panels zoom in on the time when the red and black curves diverge. For the former curves, R_p is just smaller R_cr, and for the latter $R_\mathrm{p} > R_\mathrm{cr}$. Comparing the top and the bottom panels in Fig. 10 we observe a positive feedback loop in the system in the case $R_\mathrm{p} > R_\mathrm{cr}$. When $\dot{M}_\mathrm{p}$ exceeds $\dot{M}$, the disc heats up, so the planet is irradiated with a higher temperature. This leads to a higher $\dot{M}_\mathrm{p}$, and then both increase with time above the values they would have in the disc without the planet.

Note that R_p is just a parameter controlling $\dot{M}_\mathrm{p}$ and taking the system across the FUOR ignition condition $\dot{M}_\mathrm{p} \gtrsim \dot{M}_\mathrm{b}$ in this section for the disc model chosen here. In a more general setting, $\dot{M}_\mathrm{b}$ depends on system parameters, e.g. α, M_*, and the location of the planet. There is then no fixed critical radius R_p but a range for it. A robust condition for the master mode/FUOR ignition is thus not on the planet radius but rather on the planet mass loss rate, $\dot{M}_\mathrm{p} \gtrsim \dot{M}_\mathrm{b}$, whatever the latter may be.

6.2 FUOR ignition: does a smoother transition in $\dot{M}_\mathrm{p}$ matter?

In our derivation of $\dot{M}_\mathrm{p}$ we broke the problem into two regimes, Parker wind ($R_\mathrm{B} \gg R_\mathrm{p}$, Section 5.1) and extreme evaporation ($R_\mathrm{B} < R_\mathrm{p}$, Section 5.2). This results in a discontinuous jump in $\dot{M}_\mathrm{p}$ when going from one regime to the other. A more accurate solution is likely to result in a smoother transition from Parker wind to EE. In Section 6.1 we found that FUOR ignition is a surprisingly sharp condition in terms of R_p; it was sufficient for R_p to increase by a fraction of 1 per cent above a critical value for the system to go into the self-sustained FUOR mode. One may worry that this behaviour is only due to the artificially sharp transition between the two planet mass loss regimes.

To gain an insight into how the main conclusions of our paper may depend on the idealized discontinuous transition in $\dot{M}_\mathrm{p}$ from the Parker wind to the EE model we introduce a toy 'smoothed'

Downloaded from https://academic.oup.com/mnras/article/523/1/385/7161140 by Imperial College London Library user on 17 October 2023

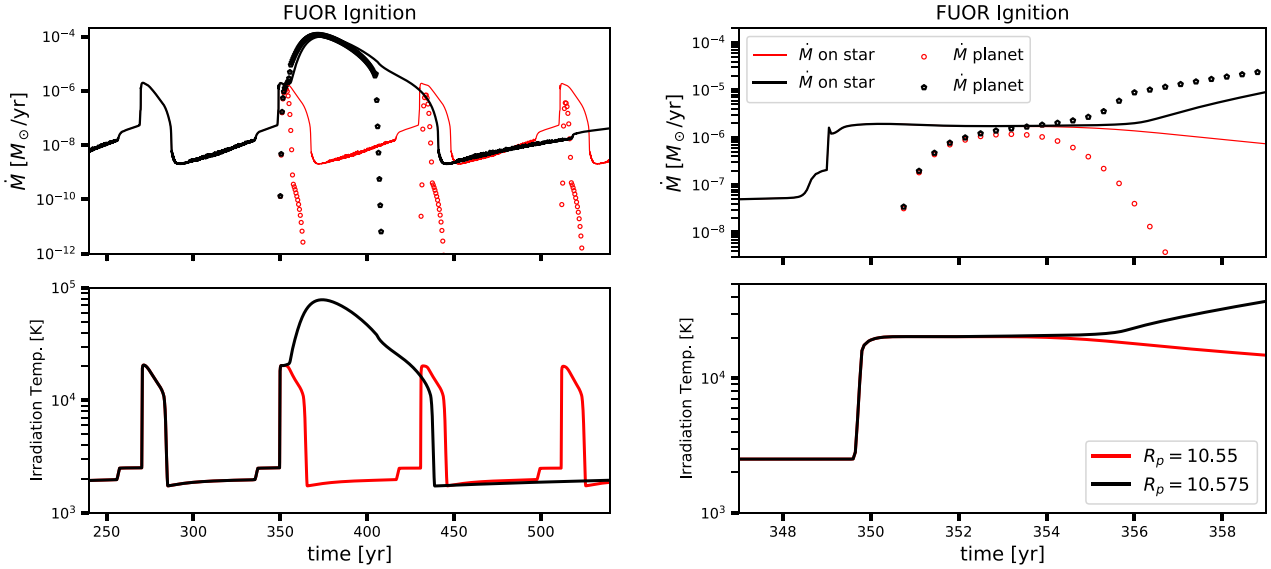


Figure 10. Idealized experiments with a planet orbiting the star at a fixed radius of 0.08 AU (Section 6.1) Note that the FUOR outburst ignites (black) when $\dot{M}_{\rm p} \gtrsim \dot{M}_*$ for a period of time, and fails to ignite (red curves) otherwise.

extreme evaporation scenario in which we use EE $\dot{M}_{\rm ee}$ for $R_{\rm B} < R_{\rm p}$, but modify $\dot{M}_{\rm p}$ in the Parker regime,

$$\dot{M}_{\rm p} = \dot{M}_{\rm se} = \begin{cases} \dot{M}_{\rm ee} \exp\left(-\frac{\Delta R}{\Delta R_{\rm tr}}\right) & \text{if } R_{\rm p} < R_{\rm B}\ , \\ \dot{M}_{\rm ee} & \text{if } R_{\rm B} < R_{\rm p} \end{cases} \tag{31}$$

Here $\Delta R = R_{\rm B} - R_{\rm p}$, and $\Delta R_{\rm tr} = \zeta R_{\rm p}$, a transition width parameter, with $\zeta = 0.25$ explored below. The respective planet mass loss rate is shown with the red dotted curve in the left-hand panel of Fig. 9 for $M_{\rm p} = 5\,{\rm M_J}$ case. Comparing the red dotted and red dashed curves we observe a significantly smoother increase in $\dot{M}_{\rm p}$ with increasing $T_{\rm h}$ in the smoothed model.

Encouragingly for our model of FU Ori, we find that despite a much more gradual increase in $\dot{M}_{\rm p}$ with $T_{\rm h}$ in the smoothed model (equation 31), the distinction between and a sharp transition between the self-sustained FUOR-like planet master and the planet slave modes remains. The left-hand panel of Fig. 11 shows two experiments with $R_{\rm p} = 8.45 R_J$ and $R_{\rm p} = 8.5 R_J$. As in Fig. 10, there is a rather different behaviour of the system for the smaller and larger planet radii, although the critical planet radius is now smaller. This could be expected. For $\Delta R_{\rm tr} = 0.25 R_{\rm p}$ and the critical planet radius of $R_{\rm cr} \sim 10.5 R_J$ found in Section 6.1, $\Delta R_{\rm tr} \sim 2.5 R_J$. We can thus expect that the FUOR ignition condition in the smoothed $\dot{M}$ model sets in at smaller radii, at $R_{\rm p} \sim R_{\rm cr} - \Delta R_{\rm tr} \sim 8\,{\rm M_J}$. We also see that FUOR ignition condition is the one on the $\dot{M}_{\rm p}$: while the critical radius changed, the $\dot{M}_{\rm p}$ at which FUOR ignition occurs did not. The right-hand panel of Fig. 11 compares the experiments with the standard and the smoothed $\dot{M}_{\rm p}$. The smoothed $\dot{M}_{\rm se}$ model results in a more gradual approach to the FUOR ignition or turn-off than the standard $\dot{M}_{\rm p}$ scenario. For example, $\dot{M}_{\rm p}$ approaches $\dot{M}_*$ earlier in the smoothed evaporation model by about 1 yr. As a result, the disc temperature in the planet's vicinity increases earlier in the $\dot{M}_{\rm se}$ model. For the same reason, the sub-critical and critical models (green and magenta colours) diverge from each other slower than the red and the black ones do.

These experiments show that (1) the existence of the self-sustained FUOR-like regime in the disc-planet system is independent of how rapidly the planet approaches EE regime; (2) planets with smaller $R_{\rm p}$ are able to power FUOR-like disc activity in the smooth EE scenario; (3) the detail of FUOR light curves produced, however, depend on the sharpness of the transition between the Parker wind and the EE regime.

6.3 A steady state or runaway planet evaporation?

Consider how the system evolves after the criterion $\dot{M}_{\rm p} \gtrsim \dot{M}$ is satisfied. For simplicity, we continue to set $R_{\rm p} = $ const. Let the disc temperature be $T_{\rm ig}$ at the point of EE ignition. As the local disc surface density rises, so does $T_{\rm h}$, and thus $\dot{M}_{\rm p}$. Due to this growth in local Σ and $T_{\rm h}$, the disc accretion rate $\dot{M}$ is increasing too. If $\dot{M}$ grows with $T_{\rm h}$ faster than does $\dot{M}_{\rm p}$, then a quasi-steady state equilibrium exists at some large $T_{\rm h} > T_{\rm ig}$ when $\dot{M}_{\rm p} \approx \dot{M}$. In that equilibrium, the disc is able to transfer the mass lost by the planet into the star. In the opposite case, if $\dot{M}$ grows with $T_{\rm h}$ slower than does $\dot{M}_{\rm p}$, then after the ignition $\dot{M}_{\rm p} > \dot{M}$ always, no matter how high $T_{\rm h}$ becomes. This will result in a runaway in $\dot{M}_{\rm p}$ and $\dot{M}$. Equation 30 shows that $\dot{M}_{\rm p} \propto T_{\rm h}^{\xi_p}$ with $\xi_{\rm p} = 2.2$. For $T > T_{\rm ig}$,

$$\dot{M}_{\rm p} = \dot{M}_{\rm p}(T_{\rm ig}) \left(\frac{T}{T_{\rm ig}}\right)^{\xi_{\rm p}} . \tag{32}$$

At the same time, steady-state one vertical zone disc equations can be solved for Kraemers' opacity $\kappa_{\rm R} = k_0 \rho T^{-7/2}$ to show that the disc midplane temperature $T \propto \dot{M}^{3/10}$, so

$$\dot{M} = \dot{M}(T_{\rm ig}) \left(\frac{T}{T_{\rm ig}}\right)^{10/3} . \tag{33}$$

This shows that an equilibrium between $\dot{M}_{\rm p}$ and $\dot{M}$ should be possible at a temperature high enough since $\xi_{\rm p} < 10/3$. Conversely, if $\xi_{\rm p} > 10/3$, no equilibrium should be possible.

In Fig. 12 we show numerical experiments set up in the same way as in Section 6.1 (Fig. 10) except that we use a fixed $R_{\rm p} = 10.6 R_J$ and $\dot{M}_{\rm p}$ as per equation (30) albeit with $\xi_{\rm p}$ different from 2.2 computed in Section 5. We observe that a quasi-steady state is reached for $\xi_{\rm p} = 2$ and $\xi_{\rm p} = 2.35$. For $\xi_{\rm p} = 2.7$ the system may be evolving towards a quasi-steady state but at such a high $\dot{M}_{\rm p}$ that

Downloaded from https://academic.oup.com/mnras/article/523/1/385/7161140 by Imperial College London Library user on 17 October 2023

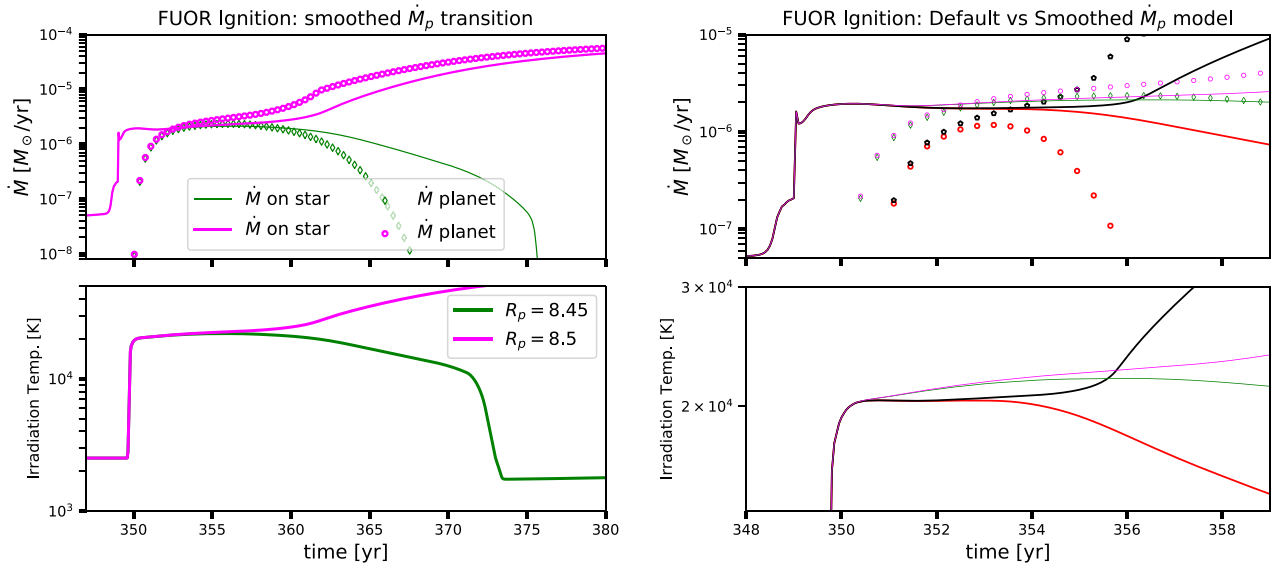


Figure 11. Left: Similar to Fig. 10, but for a smoothed transition into the extreme evaporation regime. Note that as in Fig. 10, FUOR ignition takes place above a critical R_p but not below it, albeit at smaller R_p. Right: Comparison of the standard (Fig. 10) scenario for $\dot{M}_\mathrm{p}$ with the smoothed evaporation case shown in the left-hand panel. Note that smoothed model results in a smoother transition to FUOR ignition. See Section 6.2 for detail.

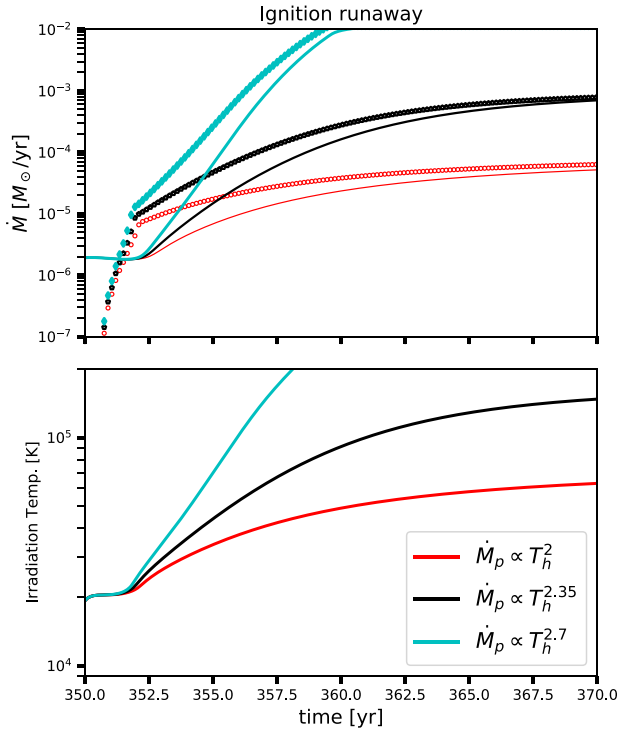


Figure 12. Same experiments as shown in Fig. 10, but for a fixed $R_\mathrm{p} = 10.6 R_J$ and varying power-law indexes ξ_p in the $\dot{M}_\mathrm{p}$ vs T_h dependence (equation 30). Note that above $\xi_p \sim 2.5$, there is no quasi-steady state in the system; the disc keeps heating up too rapidly as $\dot{M}_\mathrm{p}$ increases, driving a further increase in $\dot{M}_\mathrm{p}$, leading to a runaway.

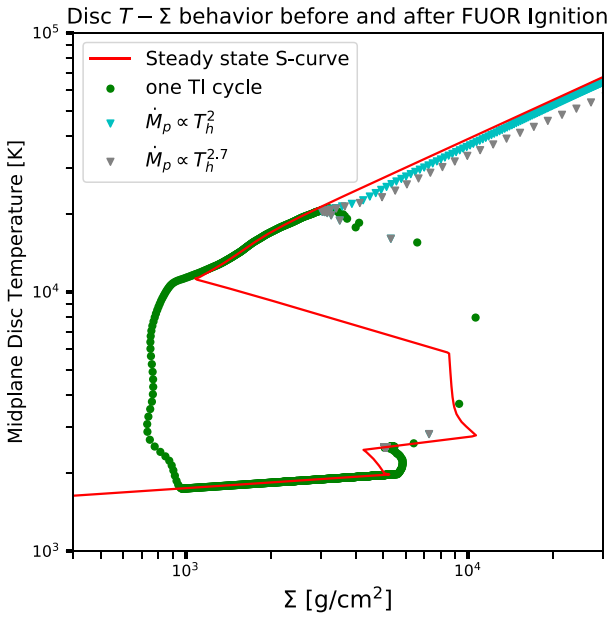


Figure 13. The track of the disc midplane T vs Σ at the location of the planet for two experiments shown in Fig. 10 is compared to the steady-state solution (the S-curve). The green circles show the disc evolution through one TI cycle before $\dot{M}_\mathrm{p}$ is turned on. The triangles show system evolution after EE ignition, when the 'unexpected' new mass supply increases local Σ and pushes the disc up the S-curve. Note that the stronger $\dot{M}_\mathrm{p}$ grows with disc temperature, the stronger it deviates from the S-curve.

many model assumptions start to break down (e.g. the disc becomes super Eddington and radiation pressure dominated). Fig. 12 thus shows that in practice, for an equilibrium $\dot{M}_*$ in the observed FUOR range, ξ_p should be significantly lower than 10/3. Fig. 13 shows the evolution of the disc at the location of the planet for the experiments from Fig. 10. This phase portrait of the disc shows yet again that the planet takes the disc above the values of T_d and Σ normally reachable in the TI cycles.

There are also constraints on the disc viscosity. The disc's viscous time at the location of the planet should be shorter than $t_\mathrm{p} = M_\mathrm{p}/\dot{M}_\mathrm{p}$, the mass loss time-scale for the planet, or else the planet will lose all of its mass before the disc is able to transfer this mass onto the star.

Downloaded from https://academic.oup.com/mnras/article/523/1/385/7161140 by Imperial College London Library user on 17 October 2023

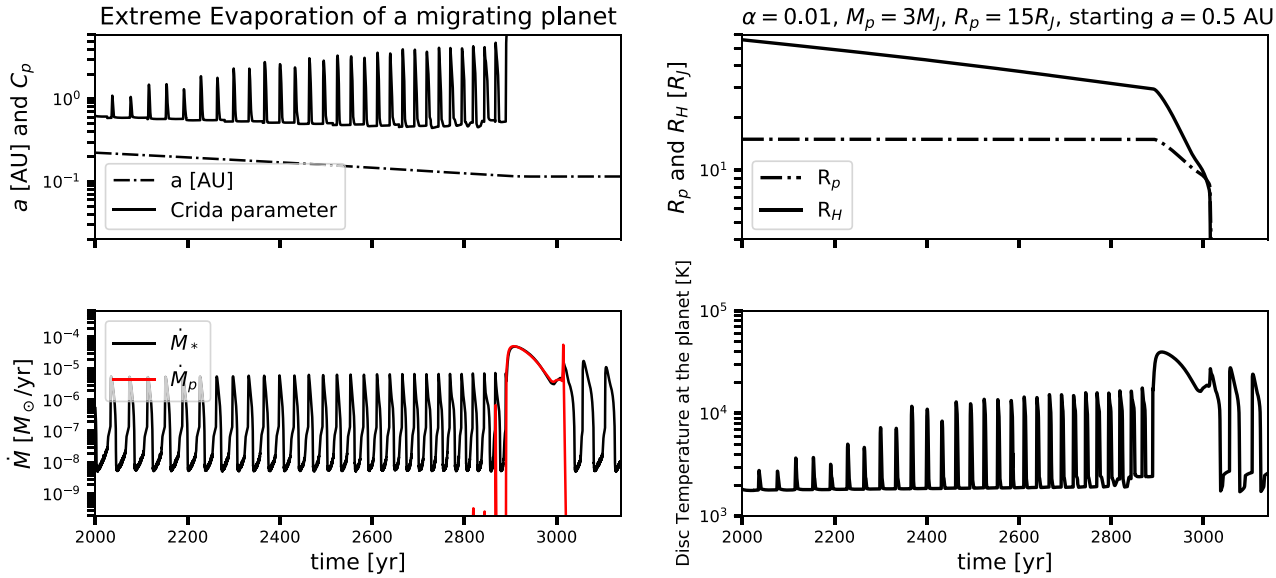


Figure 14. Evolution of the disc-planet system. separation a, planet outflow rate, accretion rate onto the star, and the hot bath (irradiation) temperature for a planet starting in a disc at $a = 0.3$ AU.

As $h = H/R \approx 0.2$ at $R = 0.08$ AU, $\alpha_h \gtrsim 10^{-3}(100\text{yr}/t_p)$. FU Ori brightened on the time-scale of $\sim$1 yr. Therefore, the disc's viscous time at the location of the planet should be no longer than a few years, that is, $\alpha_h \gtrsim$ few$\times 10^{-2}$.

6.4 A toy migrating planet example

So far in this section, a planet was held on a fixed orbit in the inner disc. Real planets, of course, must migrate into that region. From this section onward, we initiate planets far from the TI-unstable region and let them migrate radially due to tidal torques. The planet mass is evolved according to $dM_p/dt = -\dot{M}_p$. From this section the mass loss rate $\dot{M}_p$ also includes the Roche Lobe overflow (for details see section 2.2 in Nayakshin & Lodato 2012). The latter is small as long as R_p is smaller than the Hill radius, R_H, but increases very rapidly when R_p approaches R_H. What happens after FUOR ignition depends on the mass–radius relation for the planet. As it loses mass, it may expand or contract, and that may lead to significant changes in $\dot{M}_p$. Here we assume a power-law form for the mass–radius relation,

$$R_p = R_{p0}\left(\frac{M_p}{M_{p0}}\right)^{\xi_p}, \quad (34)$$

where R_{p0} and M_{p0} are the initial planet radius and mass before the mass loss sets in, and ξ_p is a dimensionless constant. For a polytropic sphere made of ionized Hydrogen with constant entropy $\xi_p = -1/3$, but we explore a range of ξ_p below.

Fig. 14 shows evolution of the disc-planet system with a $M_p = 3\,M_J$, $R_{p0} = 15R_J$ planet, with $\xi_p = 0.15$, inserted into the disc at $a = 0.5$ AU. The planet's starting position is far enough to let the disc-planet system adjust into a self-consistent albeit non-linear interaction pattern by the time extreme evaporation occurs (or not). The disc viscosity parameter is fixed at $\alpha = 10^{-2}$. The disc is fed at a steady rate $\dot{M}_{feed} = 10^{-6}M_\odot\,\text{yr}^{-1}$ at large distances. For figure clarity, we do not show the first 2000 yr of system evolution during which the planet migrated to $a \approx 0.2$ AU. The top left-hand panel of Fig. 14 shows the planet separation, a, and Crida parameter C_p (Crida, Morbidelli & Masset 2006). The planet initially migrates in the type II regime ($C_p < 1$, a deep gap in the disc is opened). This is the regime explored by Lodato & Clarke (2004). However, their planets are more massive than ours, $M_p \sim (10-15)\,M_J$ vs $M_p = 3\,M_J$ in Fig. 14, and their viscosity is lower, $\alpha = 10^{-4}$–10^{-3}. Their planets were therefore always in the type II migration regime. In contrast, as our planet nears the inner TI-unstable disc, its C_p experiences excursions into the $C_p > 1$ territory during TI flares. These excursions are due to the disc temperature (the bottom right-hand panel of Fig. 14) increasing from $\lesssim 2\times10^3$ K in quiescence to $\gtrsim 10^4$ K in TI outburst. R_H is shown in the top right-hand panel of Fig. 14. The planet is safe from TD, $R_p \ll R_H$, but it suffers EE at $a \approx 0.11$ AU. The bottom left-hand panel shows $\dot{M}_p$ with the red line. While the planet is far from the TI-unstable region, $T_h \approx 2000$ K, $\dot{M}_p$ is negligibly small. At $t = 2900$ yr, the ignition condition is satisfied, and the system enters the planet-sourced regime.

Fig. 15 zooms in onto 200 yr around the burst from Fig. 14, showing that burst with the red curve in the top panel. In addition, we also show two analogous calculations except for $\xi_p = -0.15$ and 0 for the green and black curves, respectively. As the initial radius of the planet is the same for all ξ_p, FUOR ignition occurs at the same time in the three cases. However at later times $\dot{M}_p$ and $\dot{M}_*$ evolve differently for different ξ_p. For $\xi_p = 0$, the planet radius remains constant, so $\dot{M}_p \approx$ const. For $\xi_p = -0.15$ (+0.15), the planet expands (contracts), $\dot{M}_p$ increasing (decreasing) in response. For all of the cases shown in Fig. 15, there is a strong but short spike in $\dot{M}_p$ after which it nosedives. This is TD of the planetary remnant occurring when $R_H = a(M_p/3M_*)^{1/3}$ catches up with R_p. This happens sooner for negative ξ_p, and thus the TD burst is more powerful for the green curves in Fig. 15.

7 A COMPLETE MODEL FOR FU ORI

7.1 Planet origin and properties at $R \sim 0.1$ AU

FUOR phenomenon is suspected to occur in the earliest $t \lesssim 10^5$ yr of protostellar growth (e.g. Audard et al. 2014). This is supported by the fact that discs of FUORs are 3–4 times more massive than discs in class II sources, with $\sim$2/3 of them possibly being gravitationally unstable (Kóspál et al. 2021). The only plausible source of massive

Downloaded from https://academic.oup.com/mnras/article/523/1/385/7161140 by Imperial College London Library user on 17 October 2023

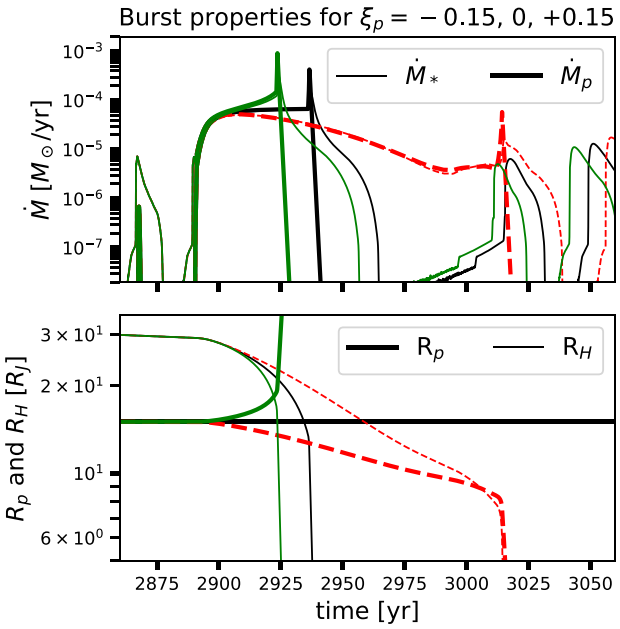


Figure 15. Same as the bottom left-hand and the top right-hand panels from Fig. 14 but three different power law indices ξ_p (see equation 34). Planets that expand when losing mass ($\xi_p < 0$) run out of mass and fill their Roche lobes sooner than planets with $\xi_p > 0$. The latter contract as they lose mass.

and extended ($R_p > 10R_J$) planets at such early times is the disc fragmentation due to GI in the outer $R \gtrsim$ tens of AU disc (e.g. Kuiper 1951; Boss 1998).

Radiative cooling constraints (Gammie 2001) show that GI planets are born very far from the inner disc, at $R \gtrsim$ tens of AU (Rafikov 2005; Rice, Lodato & Armitage 2005). Analytical estimates (Nayakshin 2010) and numerical simulations (Vorobyov & Basu 2006; Boley et al. 2010; Cha & Nayakshin 2011; Zhu et al. 2012; Vorobyov & Basu 2015; Fletcher et al. 2019) show that it can take as little as $t_I \sim 10^4$ yr for GI planets to migrate to the inner ∼few AU. This type-I-like planet migration (Baruteau, Meru & Paardekooper 2011) terminates when (depending on the planet mass and the value of the α parameter) the planets open deep gaps in the host disc and settle into the type-II regime (Fletcher et al. 2019; Humphries et al. 2019). We note in passing that these pre-collapse planets can also be tidally destroyed if they do not contract rapidly enough (see a review in Nayakshin 2017), but for FU Ori we are after planets that go through Hydrogen dissociative collapse (Bodenheimer 1974; Graboske et al. 1975).

The type II migration time-scale (e.g. Syer & Clarke 1995; Ivanov, Papaloizou & Polnarev 1999) is

$$t_{II} \sim \left(1 + \frac{M_p}{4\pi\Sigma R^2}\right) \frac{1}{\alpha\Omega h^2}\,, \tag{35}$$

where $\dot{M}_{feed} = 3\pi\alpha c_s H\Sigma$ is the disc accretion rate behind the planet far from 0.1 AU. The second term inside the brackets in equation (35) dominates in the inner disc in our model, and hence

$$t_{II} \sim \frac{M_p}{\dot{M}_{feed}} \sim 3\times10^3 \text{ yr } \frac{M_p}{3\,M_J}\,\frac{10^{-6}M_\odot yr^{-1}}{\dot{M}_{feed}}\,. \tag{36}$$

At high accretion rates, $t_{II} < t_I$, whereas at $\dot{M} \lesssim 10^{-7}M_\odot\,yr^{-1}$ the inverse is true. GI planets entering the innermost disc regions will be *at least* 10^4 yr old.

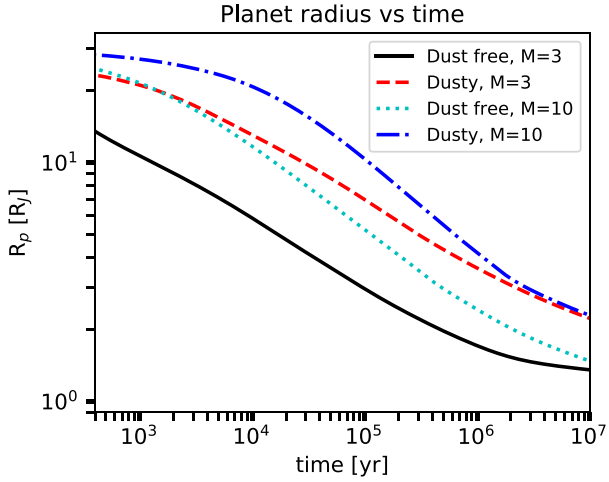


Figure 16. Radius vs time for MESA models of post-collapse giant planet contraction. Two values for planet masses are considered, along with either dust-free or dusty opacities. Planets with dusty atmospheres have radii ∼10–$20R_J$ at ages of a few 10^4 yr.

However, as mentioned previously, we are only interested in post-collapse planets as pre-collapse GI planets cannot make it into the inner 0.1 AU. The 'age' of a post-collapse planet at ∼0.1 AU is then the time it took the planet to migrate from the location at which the pre-collapse molecular clump collapsed, and this has to be beyond an 'exclusion zone'

$$R_{exc} \sim 2\text{ AU } \left[\frac{M_p}{3\,M_J}\right]^{2/3} \tag{37}$$

(e.g. see the red line in top panel of fig. 3 in Nayakshin 2016). The contraction age of post-collapse planets is therefore shorter than their age from birth at tens of AU.

What radii will these planets have when they arrive at the inner disc? Dust opacity is a major uncertainty in determining how GI planets contract, both in pre-collapse and post-collapse phases. Concerning post-collapse contraction, in particular, we estimate that dust sedimentation times in the atmospheres of $\sim 10R_J$ gas giant planets are quite short, ∼1 yr. Dust-free opacities, usually employed for post-collapse planets, thus appear reasonable. However, pebble accretion on rapidly migrating gas giant planets was found to be very efficient in numerical simulations (Boley & Durisen 2010; Humphries & Nayakshin 2018; Baehr & Klahr 2019; Forgan 2019). It can be shown that even a tiny ($\sim 10^{-4}$) fraction of that pebble accretion flux is sufficient to maintain dust opacities in the atmospheres of planets.

Therefore, we constructed MESA (Paxton et al. 2013) models of contracting gas giant planets for both dust-free and dusty atmospheres. For the latter we used dust opacity $\kappa = \kappa_0(T/1000)^b$ with constants κ_0 and b varied in a small range consistent with well known opacity calculations (such as Semenov et al. 2003; Woitke et al. 2016). In particular, κ_0 was either 3 or 6, and $b = 0.5$ or 1. We found differences of only $\lesssim$ 20 per cent in planet radius at ages of interest for all these choices, so we present here just the case $\kappa_0 = 6$ and $b = 0.5$. Density-dependent dust sublimation was modelled with the method of Kuiper et al. (2010). Fig. 16 shows evolution of R_p for $M_p = 3\,M_J$ and $10\,M_J$ that bracket the plausible range of M_p. We observe that at the planet age $10^4 \lesssim t \lesssim 10^5$ yr dust-free planets are a factor of 2 smaller than their dusty counterparts. For these ages, dusty planets have radii between $\sim 8R_J$ and $\sim 20R_J$, with $10\,M_J$ planets being larger than $3\,M_J$ planets by a factor of 1.5 or

Downloaded from https://academic.oup.com/mnras/article/523/1/385/7161140 by Imperial College London Library user on 17 October 2023

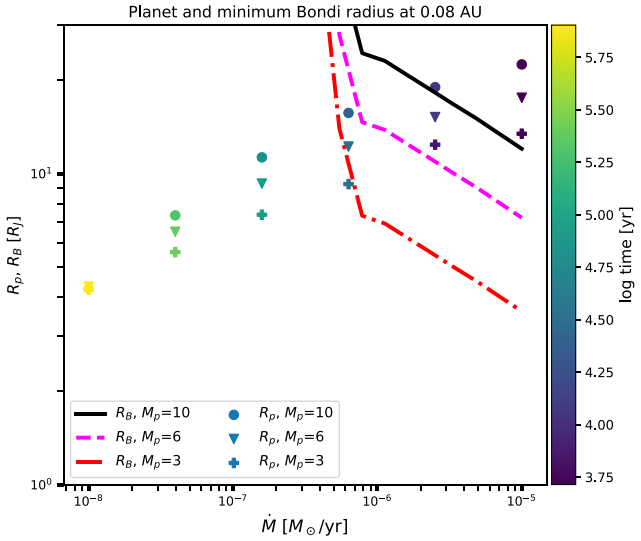


Figure 17. Planet radius (symbols) at the time it reaches $R = 0.08$ AU, and the minimum Bondi radius (lines) at that location in the disc, versus disc feeding accretion rate. This is plotted for three different values of planet masses. EE is only possible when $R_p > R_B$. This favours smaller mass planets migrating at high $\dot{M} \gtrsim 10^{-6} M_\odot$ yr^{-1} disc accretion rates.

so. This implies that on average 10 M_J planets require roughly twice hotter disc to subject them to extreme evaporation. 10 M_J planets thus must travel closer to the star to experience EE.

7.2 Constraints on disc $\dot{M}_{\rm feed}$

By using the self-consistent planet contraction tracks from Section 7.1 we can constraint the disc feeding rate $\dot{M}$ at large distances. In Fig. 17 we show experiments in which MESA models of planets of masses $M_p = 3, 6, 10\,M_J$ are injected into the disc at $R = 15$ AU. The disc is assumed to be a steady-state (Shakura & Sunyaev 1973) one fed at the rate $\dot{M}$. The planets then migrate through the disc. Simulations are stopped when the planet reaches $R = 0.08$ AU. The radius of the planet em at that time is plotted with symbols in Fig. 17 as a function of $\dot{M}$. Symbol colours convey the time it takes the planet to migrate to 0.08 AU. For each of the simulations we measure $T_{\rm max}$, the maximum disc temperature at 0.08 AU. At low $\dot{M}$, the disc is on the lower branch of the S-curve and so $T_{\rm max} \lesssim 3 \times 10^3$ K. At high $\dot{M}$ the disc is unstable to TI, and thus $T_{\rm max} \gtrsim 3 \times 10^4$ K. We use $T_{\rm max}$ to define the minimum Bondi radius,

$$R_{\rm B,min} = \frac{2GM_p\mu}{k_b T_{\rm max}} \,. \quad (38)$$

$R_{\rm B,\,min}$ is plotted in Fig. 17 with lines for different M_p.

EE of a planet at $R = 0.08$ AU occurs when $R_p \geq R_{\rm B,\,min}$. We see that at low $\dot{M}$, none of the planets can be affected by EE. The disc does not undergo TI cycles, and also, the planet takes much too long to reach the inner disc (up to 1 Myr), so it contracts too much. Additionally, more massive planets, despite being more radially extended, have a higher $R_{\rm B,\,min}$ because their gravitational potential is higher. Therefore, $M_p = 10\,M_J$ planet can only be susceptible to EE at $\dot{M} > 3 \times 10^{-6} M_\odot$ yr^{-1}. Moderately massive planets inside a high $\dot{M}$ discs can go through EE. The high $\dot{M}$ needed tallies with another requirement for the disc to be massive, i.e. to create the planet via fragmentation.

7.3 Parameter space: TD versus EE

We now explore systematically the sensitivity of the model to two major parameters, the disc feeding rate and the planet's initial mass. We ran a small grid of models in which the former was varied from $\dot{M}_{\rm feed} = 10^{-7} M_\odot$ yr^{-1} to $\dot{M}_{\rm feed} = 10^{-5} M_\odot$ yr^{-1}, and the latter from $M_p = 3\,M_J$–$10\,M_J$. We set $\xi_p = 0$, and the starting position for all the planets to $a = 10$ AU. Fig. 18 presents the most salient results: burst duration (left-hand panel), mean accretion rate during the bursts (middle panel) and the location of planet disruption (right-hand panel). The mean $\dot{M}$ shown in Fig. 18 excludes the TD spike with which the bursts end (cf. Figs 14 and 15).

The key result from Fig. 18 is the existence and a rather clean separation between the two contrasting modes of planet disruption – TD and EE. The two are separated via a diagonal line running from the bottom left corner to the top right one in all of the panels in the figure.

The top left half of the panels in Fig. 18 is filled by most massive planets migrating at all $\dot{M}_{\rm feed}$, and also by intermediate-mass planets migrating at low $\dot{M}_{\rm feed}$ – these systems tend to suffer TD, which is usually a runaway process (see section 3 in Elbakyan et al. 2021) with very intense outbursts with $\dot{M}_* \gtrsim 10^{-3} M_\odot$ yr^{-1} and duration of just a few years.

The bottom right half of the panels in Fig. 18 is taken up by 'low mass' (here $M_p \leq 4\,M_J$) planets, and also by moderately massive giants ($\sim (5-7)\,M_J$) migrating inside high $\dot{M}_{\rm feed}$ discs. These planets are exterminated by EE. The resulting accretion bursts last tens to hundreds of years with $\dot{M}_*$ from a few $\times 10^{-6} M_\odot$ yr^{-1} to $\sim 10^{-4} M_\odot$ yr^{-1}.

There is a simple reason for this dichotomy of outcomes. At a similar age, more massive planets are more compact, i.e. their M_p/R_p ratio is larger. Higher disc temperatures are needed to subject more massive planets to EE, so these planets tend to migrate closer to the star without suffering EE. However, Hill radius shrinks rapidly as planets edge closer to the star, and eventually, TDs occur before EE could occur. In terms of spatial location in the disc, TDs typically occur at $R \sim (0.03$–$0.01)$ AU. Lower-mass planets are more susceptible to EE. As they migrate towards the star, they enter EE regime while R_p is still significantly smaller than R_H. These planets evaporate in a more prolonged steady-state-like fashion, usually at distances $R \sim (0.06$–$0.2)$ AU. We discuss the TD and EE limits in particular examples below.

7.3.1 *Massive planets: short TD bursts*

Fig. 18 shows that most massive planets, $M_p \gtrsim 8\,M_J$ produce short duration (1–10 yr) bursts of exceptionally high stellar mass accretion rate, with $\dot{M}_*$ as high as $10^{-3} M_\odot$ yr^{-1}. Here we focus on a specific case of $M_p = 9\,M_J$ planet injected into a disc with $\dot{M}_{\rm feed} = 7.8 \times 10^{-7} M_\odot$ yr^{-1}. Fig. 19 shows the time close to when the planet is disrupted, which occurs at $a = 0.05$ AU. Note that planet mass loss rate is much smaller than $\dot{M}$ even during the peak TI bursts while $R_H \geq R_p$ (cf. the top right-hand panel). However, at time $t \sim 23150$ yr the opposite happens, and $\dot{M}_p$ starts to increase extremely rapidly until the planet is destroyed in a fraction of 1 yr (a zoom into the TD burst shows that $\dot{M}_*$ onto the star is slightly offset and is a little longer due to finite disc viscous time, similarly to the burst in fig. 2 in Elbakyan et al. 2021).

7.3.2 *Moderate mass planets: long FU Ori-like bursts*

In Fig. 20 we present the case of a $M_p = 4\,M_J$ injected into a disc with $\dot{M}_{\rm feed} = 3.6 \times 10^{-6} M_\odot$ yr^{-1}. The planet becomes prone to the

Downloaded from https://academic.oup.com/mnras/article/523/1/385/7161140 by Imperial College London Library user on 17 October 2023

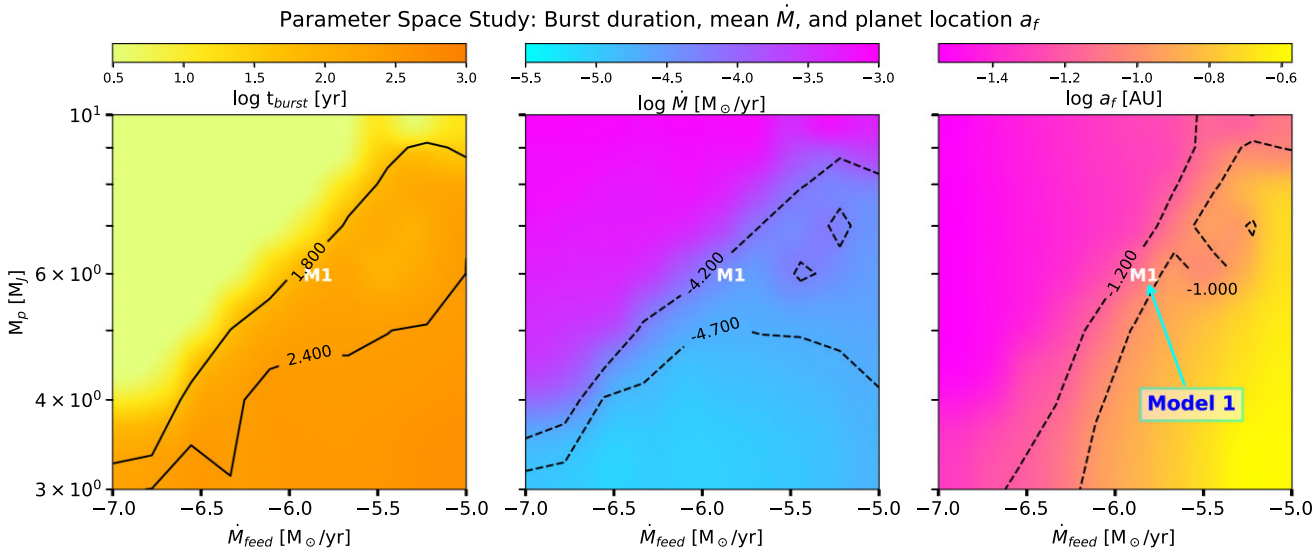


Figure 18. Parameter space study (Section 7.3) depicting burst duration (left-hand panel), mean $\dot{M}_*$ during the burst (middle panel), and location where the planet is disrupted/evaporated (right-hand panel). Symbol 'M1' marks model M1 discussed in Section 7.3.4 that appears the best match to the data. The contour lines in the panels mark the approximate region within which good models for FU Ori should be located (see text).

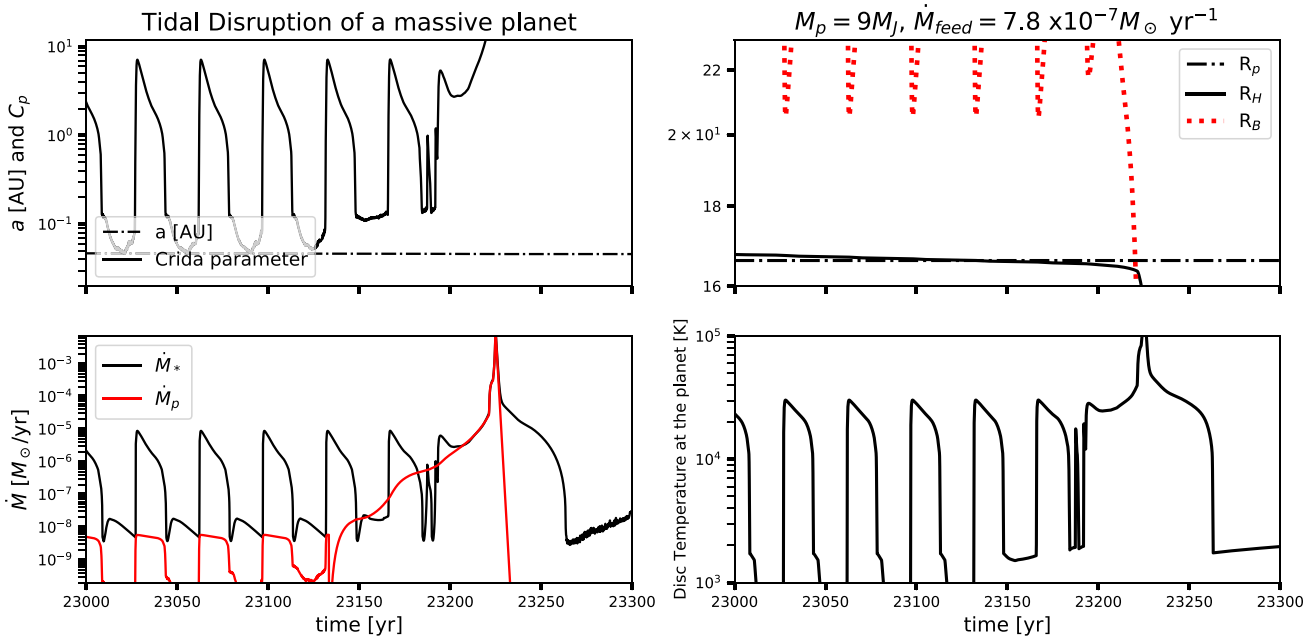


Figure 19. An example of a TD burst due to a massive $M_p = 9\,M_J$ planet. The planet is too compact to be susceptible to extreme evaporation ($R_p < R_B$), but is disrupted tidally by Roche lobe overflow. See Section 7.3.1 for detail.

EE process at time $t \approx 4520$ yr when it is at separation $a = 0.17$ AU. The top right-hand panel of Fig. 20 shows that at that time R_B drops below R_p during the TI outburst state. The resulting steady-state EE of the planet lasts for about 300 yr until its Hill radius becomes smaller than R_p. The 'last hurrah' outburst then destroys the planetary remnant in a manner discussed in Section 7.3.1.

7.3.3 A standard candle regime in EE bursts

There is a 'standard candle' regime in EE outbursts that becomes evident when we consider bursts from constant mass planets. Fig. 21 shows the planet mass loss rate for models with $M_p = 5\,M_J$ for a selection of $\dot{M}_{feed}$. We shifted the time axes so the outbursts start at $t \approx 0$. At the lowest $\dot{M}_{feed}$, the planet is in the TD regime and is hence disrupted in a few years via run-away Roche Lobe overflow (Section 7.3.1).

For all higher values of $\dot{M}_{feed}$, the burst $\dot{M}_p$ is $\sim (2-4) \times 10^{-5} M_\odot$ yr^{-1}. This is especially so for $\dot{M}_{feed} > 5 \times 10^{-7} M_\odot$ yr^{-1} cases. To understand this, note that equation (30) gives $\dot{M}_p \propto T_h^\xi R_p^{3/2}$ where $\xi \approx 2.2$. For a general case, both the disc midplane temperature, T_h, and R_p may be expected to vary significantly, so the constancy of $\dot{M}_p$ seen in Fig. 21, and a weak trend of decreasing

Downloaded from https://academic.oup.com/mnras/article/523/1/385/7161140 by Imperial College London Library user on 17 October 2023

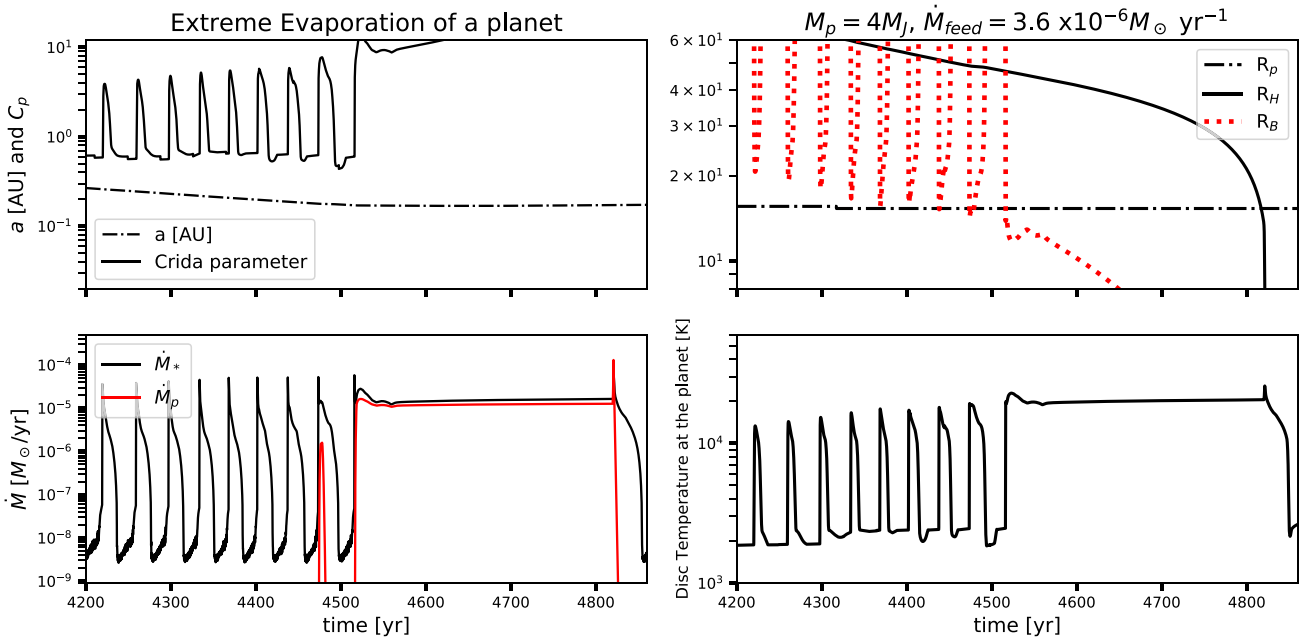


Figure 20. Same as Fig. 19 but for a less massive planet. In this case, the planet enters EE regime at $t \approx 4520$ yr and is eventually destroyed by TD at $t \approx 4830$ yr.

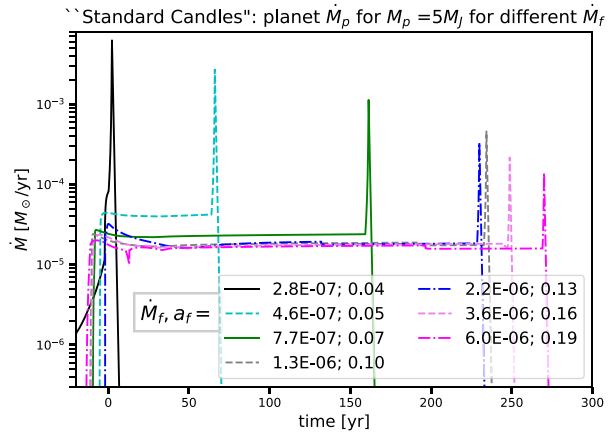


Figure 21. Planet mass loss rates for outbursts created by the destruction of planets with mass $M_\mathrm{p} = 5\,\mathrm{M_J}$ migrating through discs with different feeding rates as shown in the legend. These experiments are part of the parameter survey study shown in Fig. 18. As discussed in Section 7.3, planets in discs with low $\dot{M}_\mathrm{feed}$ are destroyed via a runaway TD (the black curve), whereas those migrating in younger discs experience a steady-state EE process. Note that $\dot{M}_\mathrm{p}$ in the latter case is nearly constant (cf. Section 7.3.3). The legend gives the disc feeding rate and the location of planet disruption in AU.

$\dot{M}_\mathrm{p}$ with increasing $\dot{M}_\mathrm{feed}$ may appear paradoxical. However, the EE evaporation sets in when R_B drops below R_p. Planet migrates in slowly *in terms of* TI cycles – generally $\sim 10^2$–10^3 TI cycles occur while planet-star separation drops by a factor of 2. Therefore, R_p is very nearly equal to R_B when EE begins (cf. the top right-hand panel in Fig. 20). It then follows that in the self-regulating system that our disc-planet system is, the mass loss rate equation (30) can be re-written as

$$\dot{M}_\mathrm{candle} = 2\times10^{-5}\frac{\mathrm{M_\odot}}{\mathrm{year}}\left(\frac{M_\mathrm{p}}{5\,\mathrm{M_J}}\right)^{2.2}\left(\frac{R_\mathrm{p}}{10R_\mathrm{J}}\right)^{-0.7}. \quad (39)$$

For a given planet mass the planet's radius varies by about a factor of 2 only when the planet's age varies by a factor of 10 (cf. Fig. 16). This explains why $\dot{M}_\mathrm{p}$ of the bursts in Fig. 21 vary so little for higher $\dot{M}_\mathrm{feed}$: their mass loss rate hovers near the 'standard candle' rate given by equation (39). This equation also explains the residual trend of decreasing $\dot{M}_\mathrm{p}$ with increasing $\dot{M}_\mathrm{feed}$ seen in Fig. 21. At higher $\dot{M}_\mathrm{p}$ the planets entering the EE regime are younger (since planet migration time is shorter at higher $\dot{M}_\mathrm{feed}$, see Section 7.1), and thus are more extended. Equation (39) predicts that the more massive the planet is, the shorter the EE outbursts, confirmed by Fig. 18.

7.3.4 *A good fit model M1*

Fig. 22 presents a model with $M_\mathrm{p} = 6\,\mathrm{M_J}$, $\dot{M}_\mathrm{feed} = 1.3\times10^{-6}\mathrm{M_\odot\,yr^{-1}}$ as the one that comes probably the closest to accounting for the observed properties of FU Ori. EE regime sets in at $a = 0.07$ AU where the orbital period is just a little short of what Siwak et al. (2018) deduce. Fig. 23 zooms in on the planet $\dot{M}_\mathrm{p}$ and star mass accretion rates. The burst has a rise time of a few years, $\dot{M}_* \sim$ few$\times10^{-5}\mathrm{M_\odot\,yr^{-1}}$, declining by about a few tens of per cent in its $\sim O(100)$ yr duration. The outburst ends with a TD of the planet when $M_\mathrm{p} = 1.4\,\mathrm{M_J}$.

7.4 The hot spot

A hot outflow from a planet is quite likely to result in a hot spot around its location. Midplane temperature in an optically thick disc, T_h, is typically a few to $\sim$10 times larger than the disc effective temperature T_eff. Normally, however, the emission of gas with T_h is inaccessible to outside observers as the disc locally shines as a blackbody at T_eff. However, an outflow from a planet may deliver hot gas to the surface of the disc in planet's vicinity. The process is unlikely to be entirely steady-state which may account for quasi-periodic nature of photometric variability (Powell et al. 2012; Siwak et al. 2018).

Downloaded from https://academic.oup.com/mnras/article/523/1/385/7161140 by Imperial College London Library user on 17 October 2023

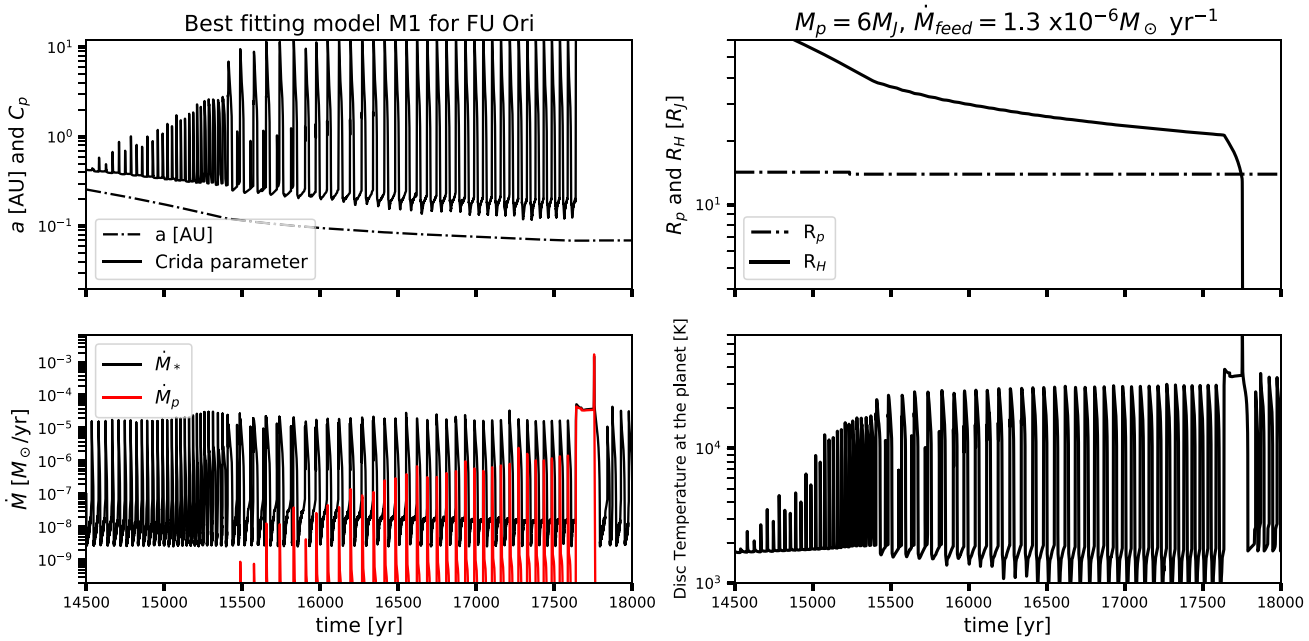


Figure 22. A 'good fit' to FU Ori, model M1 marked on Fig. 18.

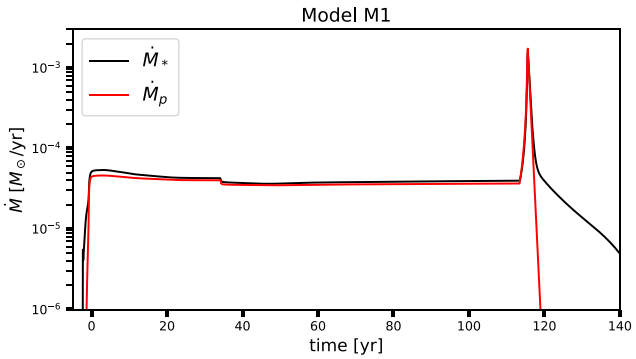


Figure 23. Planet mass loss rate and stellar accretion rates vs time for model M1 from Fig. 22.

The luminosity of the perturbation is of order the outflow's mechanical luminosity, $\Delta L \sim \dot{M}_{\rm p} c_{\rm h}^2$. Compare this with the total disc (accretion) luminosity, $L_{\rm acc} = GM_*\dot{M}_{\rm p}/R_*$, where we assume that the mass flow rate through the disc $\dot{M} \sim \dot{M}_{\rm p}$,

$$\frac{\Delta L}{L_{\rm acc}} = \frac{\dot{M}_{\rm p} c_{\rm h}^2 R_*}{GM_*\dot{M}} \sim 0.01. \tag{40}$$

Let us estimate the perturbation to the otherwise azimuthally symmetric radiation flux pattern. The unperturbed disc flux at the location of the planet is $F_0 \sim (3GM_*\dot{M}_{\rm p})/(8\pi R^3)$. Due to radiative diffusion, any point-like perturbation to the temperature structure near the disc midplane is smoothed out over an area of the size $A_p \pi H^2$, where A_p is a factor of order a few – this is the hot spot. The local enhancement of the flux is thus

$$\frac{\Delta F}{F_0} \sim \frac{\Delta L}{A_p \pi H^2 F_0} = \frac{8}{3A_p} \sim 1\,. \tag{41}$$

This is consistent with Siwak et al. (2018) estimate that the effective disc temperature deviates by ∼20 per cent in the perturbed disc region. In terms of blackbody flux, $\Delta F/F_0 = 4T_0^3 \Delta T/T_0^4 = 4\Delta T/T_0 \sim 1$, where $T_0 = T_{\rm eff}$, the unperturbed disc effective temperature.

8 DISCUSSION

We proposed that FU Ori is fed by a massive gas protoplanet located at $a \approx 0.08$ AU from the star and evaporating at an opacity-limited EE rate, calculated in Section 5. Placing a toy fixed radius non-migrating planet in a time-dependent disc (Section 6) we showed that EE process is activated during TI bursts expected to occur in young discs (Bell & Lin 1994) when disc temperatures surrounding the planet exceed $\sim 3 \times 10^4$ K. If EE mass loss rate exceeds the local disc accretion rate, then 'planet ignition' occurs. The planet becomes the dominant mass donor for the inner disc, albeit for an astrophysically short period of time.

We then built an approximate but entirely self-consistent planet-in-disc system of equations in Section 7, where the planet and disc exchange angular momentum via tidal torques, and energy and mass via EE and/or TD processes. We used MESA to calculate radius evolution for a dust-rich young planet. Moderately massive ($M_{\rm p}$ from a few to $\sim 7\,{\rm M_J}$) planets migrating in discs with $\dot{M} \gtrsim 10^{-6} {\rm M}_\odot\,{\rm yr}^{-1}$ go through a 'standard candle' EE process, producing accretion outbursts with $\dot{M}_*$ and duration similar to that of classical FUORs. For FU Ori, a small grid of models resulted in a 'good fit model' marked M1 in Fig. 18 and discussed in Section 7.3.4.

Our ideas are related to previous suggestions that TI and/or planets power FUOR events (e.g. Bell & Lin 1994; Lodato & Clarke 2004; Clarke et al. 2005; Vorobyov & Basu 2010; Nayakshin & Lodato 2012), but require both TI and planets and invoke a previously missed process (EE). Unlike many of prior studies we demand (and succeed) for our disc model to satisfy constraints on disc viscosity derived from other astronomical systems undergoing TI. We use planet migration and contraction/collapse calculations and/or constraints obtained by other authors in the context not related to FU Ori (e.g. see Nayakshin 2017 for a review). As a result, our model has very few *significant*

Downloaded from https://academic.oup.com/mnras/article/523/1/385/7161140 by Imperial College London Library user on 17 October 2023

free parameters, e.g. the grid of models in Section 7.3 only varies disc feeding rate $\dot{M}_{\rm feed}$ and $M_{\rm p}$. Yet the model satisfies a number (all that we are aware of at this time) of observational constraints:

(i) $\dot{M}$ before and during the burst are $\lesssim 10^{-7}{\rm M}_\odot\,{\rm yr}^{-1}$ and a few $\times 10^{-5}{\rm M}_\odot\,{\rm yr}^{-1}$, respectively (cf. Figs 20 and 22).

(ii) Duration of the bursts from tens to hundreds of years. See the middle panel in Fig. 18.

(iii) The observed hot spot period points at planet location $a \sim 0.08$ AU. This is naturally explained (not fine-tuned) by our model as the location where TI elicits EE of the planet. The estimated hot spot luminosity is also reasonable (Section 7.4).

(iv) The short viscous time at planet location yields outburst rise time of $\sim$1 yr, as observed (Figs 21 and 23).

(v) The size of the active disc in our model $\lesssim 0.3$ AU. For a planet located at $R \sim 0.1$ AU naturally produces an outer edge of the active disc at $\sim$(0.2–0.3) AU from the star (Figs 3–5). This is how far the material lost by the planet spreads radially in a burst of $\sim$100 yr duration (Section 3.3).

(vi) Absence of Thermal Ionization instability during FU Ori observations. The observed light curve of the source has shown a rather steady and mild decline (Clarke et al. 2005). In Section 4 we showed that this, just like the point (v) above, is naturally understood if there is a quasi-steady source of matter (a planet) in the disc interior to $\sim$0.3 AU.

(vii) Any model for FU Ori should work for $\alpha_{\rm cold} \sim 0.01$ and $\alpha_{\rm hot} \sim 0.1$ (as inferred from other TI-unstable systems, see Section 4). Our model uses these viscosity choices (Section 7).

(viii) Observations indicate that large amplitude FUOR-like events occur predominantly in massive class 0/I systems (Audard et al. 2014; Contreras Peña, Naylor & Morrell 2019), yet FU Ori's disc is somewhat an outlier in being smaller and less massive than most of FUOR discs (Kóspál et al. 2021). It may thus appear to contradict the requirement for a self-gravitating disc to be present in the system (Section 7.1). However, the physics of our model demands TI in the inner disc, which only occurs at very high $\dot{M}_{\rm feed} \gtrsim 10^{-6}{\rm M}_\odot\,{\rm yr}^{-1}$. A disc with 10 per cent of M_* would run out of fuel in less than $\sim$50 000 yr. This is comparable with the likely planet age. In addition, FU Ori's primary star is more massive and could have photo-evaporated the previously massive self-gravitating disc quite rapidly. Therefore, it is possible that FU Ori disc *was* appropriately massive when it fragmented.

(ix) It is estimated that most stars go through a dozen FUOR-like episodes spaced apart by $\sim 10^4$ yr [Hartmann & Kenyon (1996); although see Fischer et al. (2022)]. Numerical simulations show from a few to dozens of self-gravitating fragments in massive GI-unstable discs (e.g. Vorobyov & Basu 2006, 2010; Cha & Nayakshin 2011), which is sufficient to account for observations.

In the future, more detailed planet structure models should be employed. This has a potential to constrain the inner structure of very young planets via FUOR phenomenon. Coupling such models with the disc will allow a wider application of this model to other FUORs, and, potentially, to episodic accretion on high mass stars (e.g. Elbakyan et al. 2021).

ACKNOWLEDGEMENTS

SN and VE acknowledge the funding from the UK Science and Technologies Facilities Council, grant No. ST/S000453/1. JEO is supported by a Royal Society University Research Fellowship. This project has received funding from the European Research Council (ERC) under the European Union's Horizon 2020 research and innovation programme (Grant agreement No. 853022, PEVAP). This research used the ALICE High Performance Computing Facility at the University of Leicester, and DiRAC Data Intensive service at Leicester, operated by the University of Leicester IT Services, which forms part of the STFC DiRAC HPC Facility (www.dirac.ac.uk). For the purpose of open access, the authors have applied a Creative Commons Attribution (CC-BY) licence to any Author Accepted Manuscript version arising.

9 DATA AVAILABILITY

The data obtained in our simulations can be made available on reasonable request to the corresponding author.

REFERENCES

Armitage P. J., 2015, preprint (arXiv:1509.06382)
Armitage P. J., Livio M., Pringle J. E., 2001, MNRAS, 324, 705
Audard M. et al., 2014, inBeuther H., Klessen R. S., Dullemond C. P., Henning T., eds, Protostars and Planets VI, University of Arizona Press, Tucson, p.387
Bae J., Hartmann L., Zhu Z., Gammie C., 2013, ApJ, 764, 141
Bae J., Hartmann L., Zhu Z., Nelson R. P., 2014, ApJ, 795, 61
Baehr H., Klahr H., 2019, ApJ, 881, 162
Bai X.-N., Stone J. M., 2013, ApJ, 769, 76
Balbus S. A., Hawley J. F., 1991, ApJ, 376, 214
Baruteau C., Meru F., Paardekooper S.-J., 2011, MNRAS, 416, 1971
Bell K. R., Lin D. N. C., 1994, ApJ, 427, 987
Blandford R. D., Payne D. G., 1982, MNRAS, 199, 883
Bodenheimer P., 1974, Icarus, 23, 319
Bodenheimer P., Grossman A. S., Decampli W. M., Marcy G., Pollack J. B., 1980, Icarus, 41, 293
Boley A. C., Durisen R. H., 2010, ApJ, 724, 618
Boley A. C., Hayfield T., Mayer L., Durisen R. H., 2010, Icarus, 207, 509
Boss A. P., 1998, ApJ, 503, 923
Bourdarot G. et al., 2023, preprint (arXiv:2304.13414)
Burrows A. et al., 1997, ApJ, 491, 856
Cha S.-H., Nayakshin S., 2011, MNRAS, 415, 3319
Clarke C. J., Syer D., 1996, MNRAS, 278, L23
Clarke C. J., Lin D. N. C., Pringle J. E., 1990, MNRAS, 242, 439
Clarke C., Lodato G., Melnikov S. Y., Ibrahimov M. A., 2005, MNRAS, 361, 942
Coleman M. S. B., Kotko I., Blaes O., Lasota J. P., Hirose S., 2016, MNRAS, 462, 3710
Contreras Peña C., Naylor T., Morrell S., 2019, MNRAS, 486, 4590
Cowie L. L., McKee C. F., 1977, ApJ, 211, 135
Crida A., Morbidelli A., Masset F., 2006, Icarus, 181, 587
Cumming A., Butler R. P., Marcy G. W., Vogt S. S., Wright J. T., Fischer D. A., 2008, PASP, 120, 531
Davis S. W., Stone J. M., Pessah M. E., 2010, ApJ, 713, 52
Eisner J. A., Hillenbrand L. A., 2011, ApJ, 738, 9
Elbakyan V. G., Nayakshin S., Vorobyov E. I., Caratti o Garatti A., Eislöffel J., 2021, A&A, 651, L3
Fischer W. J., Hillenbrand L. A., Herczeg G. J., Johnstone D., Kóspál Á., Dunham M. M., 2022, in Inutsuka S., Aikawa Y., Muto T., Tomida K., Tamura M., eds., Protostars and Planets VII. Available at: https://authors.library.caltech.edu/114784/1/2203.11257.pdf
Fletcher M., Nayakshin S., Stamatellos D., Dehnen W., Meru F., Mayer L., Deng H., Rice K., 2019, MNRAS, 486, 4398
Forgan D. H., 2019, MNRAS, 485, 4465
Gammie C. F., 1996, ApJ, 457, 355
Gammie C. F., 2001, ApJ, 553, 174
Graboske Jr H. C., Olness R. J., Pollack J. B., Grossman A. S., 1975, ApJ, 199, 265

Downloaded from https://academic.oup.com/mnras/article/523/1/385/7161140 by Imperial College London Library user on 17 October 2023

Hameury J. M., 2020, Adv. Space Res., 66, 1004
Hameury J.-M., Menou K., Dubus G., Lasota J.-P., Hure J.-M., 1998, MNRAS, 298, 1048
Hartmann L., Kenyon S. J., 1985, ApJ, 299, 462
Hartmann L., Kenyon S. J., 1996, ARA&A, 34, 207
Herbig G. H., 1989, in Reipurth B.ed., European Southern Observatory Conference and Workshop Proceedings Vol. 33, European Southern Observatory Conference and Workshop Proceedings. p. 233
Hirose S., 2015, MNRAS, 448, 3105
Hirose S., Blaes O., Krolik J. H., Coleman M. S. B., Sano T., 2014, ApJ, 787, 1
Humphries R. J., Nayakshin S., 2018, MNRAS, 477, 593
Humphries J., Vazan A., Bonavita M., Helled R., Nayakshin S., 2019, MNRAS, 488, 4873
Ivanov P. B., Papaloizou J. C. B., Polnarev A. G., 1999, MNRAS, 307, 79
Kadam K., Vorobyov E., Regály Z., Kóspál Á., Ábrahám P., 2020, ApJ, 895, 41
King A. R., Pringle J. E., Livio M., 2007, MNRAS, 376, 1740
Kóspál Á. et al., 2021, ApJS, 256, 30
Kuiper G. P., 1951, in Hynek J. A., ed., 50th Anniversary of the Yerkes Observatory and Half a Century of Progress in Astrophysics, 37 National Academy of Sciences, USA, p. 357
Kuiper R., Klahr H., Beuther H., Henning T., 2010, ApJ, 722, 1556
Labdon A. et al., 2021, A&A, 646, A102
Lasota J.-P., 2001, New Astron. Rev., 45, 449
Lasota J. P., Dubus G., Kruk K., 2008, A&A, 486, 523
Lesur G. R. J., 2021, A&A, 650, A35
Lodato G., Clarke C. J., 2004, MNRAS, 353, 841
Lykou F. et al., 2022, A&A, 663, A86
Meyer F., Meyer-Hofmeister E., 1984, A&A, 132, 143
Mori S., Bai X.-N., Okuzumi S., 2019, ApJ, 872, 98
Nayakshin S., 2010, MNRAS, 408, L36
Nayakshin S., 2016, MNRAS, 461, 3194
Nayakshin S., 2017, PASA, 34, e002
Nayakshin S., Lodato G., 2012, MNRAS, 426, 70
Nayakshin S., Elbakyan V., Rosotti G., 2022, MNRAS, 512, 6038
Owen J. E., Wu Y., 2016, ApJ, 817, 107
Paxton B. et al., 2013, ApJS, 208, 4
Pérez S. et al., 2020, ApJ, 889, 59
Powell S. L., Irwin M., Bouvier J., Clarke C. J., 2012, MNRAS, 426, 3315
Rafikov R. R., 2005, ApJ, 621, L69
Rice W. K. M., Lodato G., Armitage P. J., 2005, MNRAS, 364, L56
Santerne A. et al., 2016, A&A, 587, A64
Semenov D., Henning T., Helling C., Ilgner M., Sedlmayr E., 2003, A&A, 410, 611
Shakura N. I., Sunyaev R. A., 1973, A&A, 24, 337
Simon J. B., Beckwith K., Armitage P. J., 2012, MNRAS, 422, 2685
Siwak M. et al., 2018, A&A, 618, A79
Smak J., 1984, AcA, 34, 161
Suzuki T. K., Ogihara M., Morbidelli A., Crida A., Guillot T., 2016, A&A, 596, A74
Syer D., Clarke C. J., 1995, MNRAS, 277, 758
Tabone B., Rosotti G. P., Cridland A. J., Armitage P. J., Lodato G., 2021, MNRAS, 512, 2290
Vazan A., Helled R., 2012, ApJ, 756, 90
Vorobyov E. I., Basu S., 2005, ApJ, 633, L137
Vorobyov E. I., Basu S., 2006, ApJ, 650, 956
Vorobyov E. I., Basu S., 2010, ApJ, 719, 1896
Vorobyov E. I., Basu S., 2015, ApJ, 805, 115
Woitke P. et al., 2016, A&A, 586, A103
Zhu Z., Hartmann L., Calvet N., Hernandez J., Muzerolle J., Tannirkulam A.-K., 2007, ApJ, 669, 483
Zhu Z., Hartmann L., Calvet N., Hernandez J., Tannirkulam A.-K., D'Alessio P., 2008, ApJ, 684, 1281
Zhu Z., Espaillat C., Hinkle K., Hernandez J., Hartmann L., Calvet N., 2009a, ApJ, 694, L64
Zhu Z., Hartmann L., Gammie C., 2009b, ApJ, 694, 1045
Zhu Z., Hartmann L., Gammie C., McKinney J. C., 2009c, ApJ, 701, 620
Zhu Z., Hartmann L., Gammie C., 2010, ApJ, 713, 1143
Zhu Z., Hartmann L., Nelson R. P., Gammie C. F., 2012, ApJ, 746, 110
Zhu Z., Jiang Y.-F., Stone J. M., 2020, MNRAS, 495, 3494

This paper has been typeset from a TEX/LATEX file prepared by the author.

Downloaded from https://academic.oup.com/mnras/article/523/1/385/7161140 by Imperial College London Library user on 17 October 2023

© 2023 The Author(s)
Published by Oxford University Press on behalf of Royal Astronomical Society. This is an Open Access article distributed under the terms of the Creative Commons Attribution License (https://creativecommons.org/licenses/by/4.0/), which permits unrestricted reuse, distribution, and reproduction in any medium, provided the original work is properly cited.